Monthly Notices
of the
ROYAL ASTRONOMICAL SOCIETY

MNRAS **468,** 1575–1593 (2017)
Advance Access publication 2017 February 20

doi:10.1093/mnras/stx428

Deposition of steeply infalling debris around white dwarf stars

John C. Brown,[1] Dimitri Veras[2]★ and Boris T. Gänsicke[2]

[1]*School of Physics and Astronomy, University of Glasgow, Glasgow G12 8QQ, UK*
[2]*Department of Physics, University of Warwick, Coventry CV4 7AL, UK*

Accepted 2017 February 16. Received 2017 February 9; in original form 2016 November 17

ABSTRACT

High-metallicity pollution is common in white dwarf (WD) stars hosting remnant planetary systems. However, they rarely have detectable debris accretion discs, possibly because much of the influx is fast steeply infalling debris in star-grazing orbits, producing a more tenuous signature than a slowly accreting disc. Processes governing such deposition between the Roche radius and photosphere have so far received little attention and we model them here analytically by extending recent work on sun-grazing comets to WD systems. We find that the evolution of cm-to-km size (a_0) infallers most strongly depends on two combinations of parameters, which effectively measure sublimation rate and binding strength. We then provide an algorithm to determine the fate of infallers for any WD, and apply the algorithm to four limiting combinations of hot versus cool (young/old) WDs with snowy (weak, volatile) versus rocky (strong, refractory) infallers. We find: (i) Total sublimation above the photosphere befalls all small infallers across the entire WD temperature ($T_{\rm WD}$) range, the threshold size rising with $T_{\rm WD}$ and 100× larger for rock than snow. (ii) All very large objects fragment tidally regardless of $T_{\rm WD}$: for rock, $a_0 \gtrsim 10^5$ cm; for snow, $a_0 \gtrsim 10^3$–3×10^4 cm across all WD cooling ages. (iii) A considerable range of a_0 avoids fragmentation and total sublimation, yielding impacts or grazes with cold WDs. This range rapidly narrows with increasing $T_{\rm WD}$, especially for snowy bodies. Finally, we briefly discuss how the various forms of deposited debris may finally reach the photosphere surface itself.

Key words: methods: numerical – celestial mechanics – minor planets, asteroids: general – planets and satellites: dynamical evolution and stability – protoplanetary discs – white dwarfs.

1 INTRODUCTION

The stratification of white dwarf (WD) atmospheres by atomic weight provides a tabula rasa upon which any deposited contaminants conspicuously stand out. Abundant contaminants, in the form of heavy metals, have now been observed in one-quarter to one-half of all WDs (Zuckerman et al. 2003, 2010; Koester, Gänsicke & Farihi 2014). These metals cannot represent relics from stellar evolution because their diffusion (sinking) time-scales are orders of magnitude shorter (Paquette et al. 1986; Wyatt et al. 2014) than the age of the WDs (the *cooling time*). The metals also cannot have predominantly arisen from the interstellar medium, which is too rarefied and hydrogen rich (Aannestad et al. 1993; Friedrich, Jordan & Koester 2004; Jura 2006; Kilic & Redfield 2007; Farihi et al. 2010).

Instead, the metals must originate from planetary system remnants (Gänsicke et al. 2012; Jura & Young 2014; Xu et al. 2014; Farihi et al. 2016; Melis & Dufour 2017). This exciting development has been bolstered by strong evidence of at least one asteroid disintegrating in real time around a WD (Vanderburg et al. 2015; Alonso et al. 2016; Gänsicke et al. 2016; Rappaport et al. 2016; Redfield et al. 2016; Xu et al. 2016; Zhou et al. 2016; Gary et al. 2017; Gurri, Veras & Gänsicke 2017; Veras et al. 2017a) as well as nearly 40 dusty and gaseous discs orbiting within a distance of about one solar radius (Zuckerman & Becklin 1987; Gänsicke et al. 2006, 2008; Farihi, Jura & Zuckerman 2009; Wilson et al. 2014; Barber et al. 2016; Dennihy et al. 2016; Farihi 2016; Manser et al. 2016a,b). However, of the ∼1000 metal polluted WDs known, these 40 harbouring discs represent only a few per cent.

Hence, a key question is how such WDs without detectable discs become polluted? This pressing question has received little theoretical attention (Veras 2016a) but it would seem likely either that the slowly infalling flat dense disc is too tenuous for detection or that the infall is substantially attributable to high-speed steep infall of tenuous matter in near-parabolic orbits of periastron distances near the stellar radius, and possibly is fairly isotropic. Simulations have shown that both grazing encounters (Mustill, Veras & Villaver 2014; Veras & Gänsicke 2015; Hamers & Portegies Zwart 2016; Veras et al. 2016; Veras 2016b; Petrovich & Muñoz 2017) and even direct stellar impacts (Veras et al. 2013, 2017b,c) should occur.

★ E-mail: d.veras@warwick.ac.uk

These encounters and potential impacts can include comets (Alcock, Fristrom & Siegelman 1986; Veras, Shannon & Gänsicke 2014b; Stone, Metzger & Loeb 2015), asteroids (Bonsor, Mustill & Wyatt 2011; Debes, Walsh & Stark 2012; Frewen & Hansen 2014; Antoniadou & Veras 2016) or even small moons (Payne et al. 2016, 2017) though, as we show in this paper, these will become tidally fragmented nearer the star. Icy bodies like minor planets could easily retain internal water during the giant branch stages of evolution (Jura & Xu 2010, 2012; Malamud & Perets 2016), so continued consideration of such bodies and even weaker snowy ones like comets is important. The simulations in none of the above papers, however, described the physical details of the encounters, and just a handful of studies have considered physical aspects of the problem of destruction of bodies undergoing near-direct infall towards WD stars (Alcock et al. 1986; Bear & Soker 2015; Stone et al. 2015).

Here, we approach the problem of near-direct infall from a different perspective, by building on the analysis of the destruction regimes of steeply infalling solar comets by Brown et al. (2011) and Brown, Carlson & Toner (2015). They consider both sublimation by starlight (at r near $\mathrm{R}_\odot$) and bow-shock ablation and ram pressure effects. Here, we extend their analysis to: (i) the much larger range of parameters involved when one includes hard rocky infalling bodies; (ii) the very different stellar parameters of WD stars and (iii) the tidal fragmentation regime (which Brown et al. 2011 and Brown et al. 2015 mostly ignored) because WD surface gravity is much stronger than solar gravity. Our aim is to determine (analytically and numerically) for what parameters the destruction of bodies of different sizes and properties is dominated by different processes, and the implications for WD pollution.

The primary goals of this paper are to: (i) elucidate the physics of steep infall of small bodies towards WDs; and (ii) develop a useful algorithm for determining the outcomes. In the following two sections, we discuss the meaning, importance, range and uncertainty of values of all relevant WD stars (Section 2) and small body (Section 3) parameters. In Section 4, we describe the various relevant debris destruction processes – sublimation, fragmentation and grazing/impacts, and in Section 5 we analyse which process(es) dominate in what spatial regime as a function of the parameters of the WD star and infalling object. We defer to Section 6 a discussion of the physics of debris impacting the photosphere directly. Then, in Section 7, we summarize our conclusion (7.1) and briefly discuss issues that need attention as to how debris (other than direct impactors) can finally reach the WD surface for the cases of sublimated matter, fragmented matter (where tides exceed strength) and steep star grazers (near misses) orbiting the WD.

In order to aid the reader, we have summarized the meaning and location of the most important variables in Tables 1 and 2.

2 WHITE DWARF (WD) STAR PROPERTIES

2.1 WD masses and radii

It is well known that WD stars occupy only a narrow range of masses $M_{\rm WD}$ because remnant WD masses much above 1 $\mathrm{M}_\odot$ need rather large (so rare) progenitor masses while WDs of much below 1 $\mathrm{M}_\odot$ are not reached by evolution within the current age of the Universe. Here, we will consider WDs in the mass range 0.4–0.8 $\mathrm{M}_\odot$ and in many of our results we use a mean value of 0.6 $\mathrm{M}_\odot$ (Liebert, Bergeron & Holberg 2005; Falcon et al. 2010; Tremblay et al. 2016). The range of WD radii $R_{\rm WD}$ is even smaller because of the form of the mass–radius relationship (Hamada & Salpeter 1961) set mainly by the hydrostatic balance of gravity and electron degeneracy pressure. For this, we recognize that the relation is approximately independent of temperature over a wide range (Panei, Althaus & Benvenuto 2000)[1] and use the approximation.

$$R_\star = \gamma \mathrm{R}_\odot \left[\frac{M_\star}{\mathrm{M}_\odot}\right]^{-1/3}, \tag{1}$$

where

$$\gamma \simeq 10^{-2}. \tag{2}$$

2.2 WD ages and effective temperatures

WDs form with very high temperatures and cool at first very fast, but with rapidly decreasing rates by blackbody radiation. Their effective surface temperatures $T_{\rm WD}$ are an easily observed quantity, physically fixed by the cooling age $\tau_{\rm WDcool}$ of the star. The relationship between $\tau_{\rm WDcool}$ and $T_{\rm WD}$ also weakly involves $M_{\rm WD}$ and has been studied in detail by Mestel (1952), D'Antona & Mazzitelli (1990), Bergeron, Wesemael & Beauchamp (1995) and Fontaine, Brassard & Bergeron (2001), but the following is an adequate rough approximation here.

$$\tau_{\rm WDcool} \approx 700\,\mathrm{Myr}\left(\frac{T_{\rm WD}}{10^4\,\mathrm{K}}\right)^{-b}, \tag{3}$$

where $b \sim 4.5$.

2.3 Other WD quantities defined by mass and temperature

The quantities ($M_{\rm WD}$, $T_{\rm WD}$) are sufficient to define the following quantities which also arise in our modelling. The WD bolometric luminosity and radiation flux at asterocentric distance r are (with $x = r/R_\star$)

$$F_{\rm rad}(r) = \frac{L_\star}{4\pi r^2} = \left[\frac{R_\star}{r}\right]^2 \sigma T_\star^4 = \frac{F_\star}{x^2} \tag{4}$$

while the WD surface gravity is

$$g_\star = \frac{GM_\star}{R_\star^2}, \tag{5}$$

where σ and G are the Stefan–Boltzmann and Universal Gravitation constants. Likewise the surface escape speed $v_\star = (2GM_\star/R_\star)^{1/2}$ which, for the WD case, becomes $v_\star = v_\odot \gamma^{-1/2}(M_\star/\mathrm{M}_\odot)^{2/3}$.

2.4 WD atmospheres

In the case of (grazing) infallers that are both large enough in size and small enough in periastron distance q to reach the dense inner layers of the atmosphere, fluid interactions take over from radiation and tides and the density structure $\rho_{\rm a}(r)$ of the atmosphere determines the destruction depth. For this case, we will use a locally exponential model $\rho_{\rm a}(r) = \rho_{\rm a0}\exp(-z/H)$ of constant scaleheight H with $z = r - R_{\rm WD}$. We will take the hydrostatic scaleheight to be that for ionized hydrogen (atomic mass $m_{\rm p}$) at the WD effective temperature, viz

$$H = \frac{2kT_{\rm WD}}{m_{\rm p} g_{\rm WD}} \tag{6}$$

[1] More precise, but analytically less tractable relations, can be found in equations (4) and (5) of Veras et al. (2014a).

Table 1. Some Roman variables and parameters used in this paper.

Variable	Explanation	Equation number(s)
A	Sublimation parameter (cm)	13, 15–20
a	Mean dimension of infaller	11, 14, 26, 29
a_0	Initial infaller a value	
$a_{0\mathrm{crit}}$	$a(x)$ at which $a_{\mathrm{sub}} = a_{\mathrm{frag}}$	
a_{frag}	Size for fragmentation onset	29
a_{sub}	Sublimated radius (at x)	11
B	Binding parameter (cm)	30, 34–39
C_{H}	Bow shock to nucleus heat transfer coefficient	
$\mathcal{E}$	Nucleus kinetic energy at impact	
f_{cross}	Function which defines x, if any, at fragmentation onset	41
F_{ab}	Ablative energy flux	
F_*	Bolometric radiation flux at star surface	
F_{rad}	Bolometric radiation flux at r	4
$\mathcal{F}_{\mathrm{tot}}$	Net disruptive force	21
$\mathcal{F}_{\mathrm{T}}$	Tidal force	22
$\mathcal{F}_{\mathrm{G}}$	Self-gravity binding force	23
$\mathcal{F}_{\mathrm{S}}$	Tensile strength force	24
G	Gravitational constant	
g_*	Stellar surface gravity	5
H	Density scaleheight	6
k	Boltzmann constant	
L_*	Bolometric stellar luminosity	
$\mathcal{L}$	Latent heat of 'vaporization'	
M	Infaller mass	7, 12
M_*	Stellar mass	
M_0	Initial stellar mass	
m_{p}	Proton mass	
$n_{\mathrm{a}}^{\mathrm{subtoab}}$	Stellar atmosphere hydrogen number density	
$\mathcal{P}$	Instantaneous power of energy released in impact	
P_{ram}	Ram pressure of atmosphere impinging on infaller	
P_{ramsub}	Ram pressure of sublimating mass outflow	
q	Infaller periastron distance	
Q	Total vaporization energy for ablation	
R	Stellar radius	1
$\mathcal{R}$	Ratio of self-gravity to material strength	31–33
r	Astrocentric distance of infaller	
S	Infaller's tensile strength	
Δt	Time-scale of impact energy deposition	
T	Stellar effective temperature	
v_*	Escape speed from stellar surface	
$v(r)$	Infaller speed	9
X	$\equiv 2Q/C_{\mathrm{H}}v_\star^2$	
x	$\equiv r/R_\star$	
x_1, x_2	The real solutions of equation (41), if any	
x_{crit}	The x value at which $a_{\mathrm{sub}} = a_{\mathrm{frag}}$	42
x_{sub}	The x value where total sublimation occurs for a size a_0	
x_{Roche}	The x value at the Roche radius	28
X_{-2}	$=100X$	

while the reference surface density can be fitted to more realistic WD model atmosphere results such as those of Tremblay et al. (2011, 2013, 2015).

For generality below, we will first derive debris destruction equations for stars of any ($M_\star$, $R_\star$, $T_\star$) including the solar case ($\mathrm{M}_\odot, \mathrm{R}_\odot, \mathrm{T}_\odot$) and then from them derive those for the WD case as a function of (M_{WD}, T_{WD}) using the mass–radius relationship (1). We do not concern ourselves here with variations in properties among the different classes of WDs because the large uncertainty and range in the infalling bodies (especially their strength) is much larger and dominates the uncertainties in our results.

3 PROPERTIES OF INFALLING BODIES

3.1 Introduction

In this section, we will mainly be defining terminology and discussing typical values of properties of individual infalling bodies. We adopt homogeneous mean values through the body volume as reasonable – i.e. we consider the bodies to have individual *integrity* in the way one would normally think of an asteroid, rock, pebble or hard-packed dirty snowball. However, we recognize that many debris objects have only limited integrity, especially when it comes to strength, such as loose ice/snow/dust/rock conglomerates and

Table 2. Some Greek variables and parameters used in this paper.

Variable	Explanation	Equation number(s)
α	$\equiv A/a_0$	40
β	$\equiv B/a_0$	40
Γ	$\equiv 3^{1/4} + 3^{-3/4}$	44
γ	$\equiv 10^{-2}$ (WD radius factor)	2
θ	Impactor entry angle to vertical	
μ	$\equiv \cos\theta$	
ρ	Infaller mass density	
$\rho_{\rm a}$	Atmospheric mass density	55, 57
$\rho_{\rm a}^{\rm subtoab}$	Atmospheric mass density crossover point from sublimation to ablation dominated	
σ	Stefan–Boltzmann constant	
Σ	Vertical atmospheric column mass density	54, 56

inhomogeneous rocks containing cavities, cracks etc. – or uncemented rubble piles or sand heaps held together with almost exclusively self-gravity. For these, it is essential to recognize the internal inhomogeneity of parameter values and its consequences. For example, for a body made almost entirely of hard rock, but permeated by cracks or surfaces of weakness, the local *strength* of the rock material itself against strains is far higher than the effective strength of the body as a whole. Related is the ease or difficulty of pulling it apart into smaller stronger bodies of greater integrity – i.e. strength exceeding self-gravity. This important distinction will arise especially in Sections 3.5 and 4.3.

3.2 Nucleus shape and size

We know from direct imaging, and from light curve data, that cometary nuclei and asteroids are of diverse, irregular and distinctly aspherical shapes. For our modelling purposes, therefore we characterize their linear size by a single mean dimension a, their volume as a^3 and their direction-averaged cross-sectional area as a^2. If the shape were actually spherical with radius $a_{\rm s}$ and we chose $a = 1.65a_{\rm s}$ then our expressions for the volume and the cross-section would differ from the true values only by $\sim$10 per cent. We define the initial size $a_0 \equiv a(r \to \infty)$, where $a(r)$ is its value at asterocentric distance r.

3.3 Density ρ and mass $M(r)$

We approximate the mass density ρ – and other intrinsic properties (e.g. S, $\mathcal{L}$, see below) – of the infalling body as being uniform throughout its volume. Then the body's constant density ρ, and its evolving mass $M(r)$ and size $a(r)$ at r are related – provided it does not change shape or fragment – by

$$M(r) = \rho a^3(r). \tag{7}$$

The mean value widely used for the density of cometary objects is around half that of water (1 g cm^{-3}) but values vary somewhat between objects and estimates. They are thought to be comprised of a porous mix of ices, dust and rubble (*dirty snowball*) which in this paper, for brevity, we will loosely term *snow*. Here, we allow for this variation by using a fiducial value $\rho_{\rm snow} = 0.5$ g cm^{-3} and writing the actual $\rho = \rho_{\rm snow} \times [\rho/\rho_{\rm snow}]$ when dealing with comet-like material with the dimensionless factor in square brackets selectable in a range of say 0.3–3.

Solid bodies like asteroids and pebbles (including solid ice) are denser, with ρ in the range from around 1 g cm^{-3} for solid ices to $\sim$10 g cm^{-3} for bodies rich in iron ($\rho \simeq 8$ g cm^{-3}) and heavier materials. We therefore define a fiducial value used in numerical expressions of $\rho_{\rm rock} = 3$ g cm^{-3} and writing $\rho = \rho_{\rm rock} \times [\rho/\rho_{\rm rock}]$ when dealing with rocky material with the dimensionless factor in square brackets again selectable in a range of say 0.3–3.

3.4 Latent heat $\mathcal{L}$

The intrinsic parameters of an infalling body which mainly determine its rate of mass-loss per unit area for a specified heating flux per unit area (see Section 4) are its density ρ and latent heat $\mathcal{L}$ of sublimation/ablation. The relevant values of $\mathcal{L}$ for a star-grazing ice-conglomerate snowy mix for the regimes of intense heating where all components are vaporized was taken by (Brown et al. 2011, in their section 2.2.2) to be the density-weighted mean over all mass components, including volatile and refractory ones, which for a typical snowy cometary nucleus is $\mathcal{L}_{\rm snow} \approx \mathcal{L} = 2.6 \times 10^{10}$ erg g^{-1}. For solid rocky materials, $\mathcal{L}$ is a few times higher: e.g. Chyba, Thomas & Zahnle (1993) adopted 2.3×10^{10} erg g^{-1} for comets, 8×10^{10} erg g^{-1} for stony/iron bodies and 10^{11} erg g^{-1} for solid iron.

To allow for this range of values in both the snowy and rocky regimes, we proceed similarly to what we did in subsection 3.2 for densities and write $\mathcal{L} = \mathcal{L}_{\rm snow} \times [\mathcal{L}/\mathcal{L}_{\rm snow}]$ for snowy objects and $\mathcal{L} = \mathcal{L}_{\rm rock} \times [\mathcal{L}/\mathcal{L}_{\rm rock}]$ for rocky objects with fiducial values in numerical expressions of $\mathcal{L}_{\rm snow} = 2.6 \times 10^{10}$ erg g^{-1} and $\mathcal{L}_{\rm rock} = 8 \times 10^{10}$ erg g^{-1} where the square-bracket factors again are selectable in a range of say 0.3–3.

Note that some of our equations below involve the product $\rho\mathcal{L}$ which, for the above fiducial values, is about 20 times larger for rock than for snow. This in itself can be expected to yield very different behaviours of these two types of debris, but the difference in strength S is even more dramatic as we now see.

3.5 Strength S

In addition to sources of heat driving mass-loss, infalling bodies experience disruptive forces that can contribute to their dissipation both directly and by accelerating their mass-loss. These forces include: (i) the radial *tensional* tidal force (gravity gradient) of the WD star; (ii) the associated azimuthal *shear* force (from the orbital speed gradient; Davidsson 1999, 2001); (iii) for bodies that enter the dense inner atmosphere of the WD (Brown et al. 2011, 2015), the *compressional* force from the gradient of the ram pressure of the interaction with the dense atmosphere, and the lift force in the case of very shallow angle incidence; (iv) stellar radiation pressure that can be important compared to gravity for dust particles. For the larger primary infalling bodies considered here ($a_0 > 1$ cm), this

Table 3. Our fiducial intrinsic parameter values for infalling objects.

Type	Density ρ (g cm^{-3})	Latent Heat $\mathcal{L}$ (erg g^{-1})	Tensile strength S (dyne cm^{-2})
Rock	3.0	8.0×10^{10}	10^{10}
Snow	0.5	2.6×10^{10}	10^{4}

resulting force can be neglected, especially in the very strong gravity of WDs; and possibly (v) the pressure gradient force arising from very intense sublimative mass outflow (Sekanina & Kracht 2015). We will, however, return to the matter of radiation pressure when we briefly consider in Section 7 the final stage of arrival at the star of the much smaller debris (dust and atoms) created by sublimation and fragmentation.

The effects of these forces on the body depends on the ability of its material to resist them, i.e. its relevant *strengths: tensile, shear, compressive*. Across the diverse infalling material properties, these strengths S are the most wide-ranging in value. The different *types* of strength can also differ considerably from each other for a single material but less so than the variation of a specific strength (e.g. tensile) between materials, so here we will solely use tensile S values as a starting point.

Consider for example, the mean local tensile strength S which (together with self-gravity) resists the disruptive tidal gravity gradient. This can be as high as a few times 10^{10} dyne cm^{-2} for uniformly hard rocks (like granite). For comparison, the mean tensile strength value for the loose ice-conglomerate of some cometary nucleus material has been estimated from modelling and lab measurements to be possibly as low as 10^{3} dyne cm^{-2} (see e.g. Greenberg, Hitoshi & Tetsuo 1995, Gundlach & Blum 2016 and references therein). A range of 10^{3}–10^{7} dyne cm^{-2} has been reported for the localized surface strengths of Comet 67P/Churyumov–Gerasimenko by Biele et al. (2015) from two of the bounces of ESA's Rosetta Philae lander but the strength relevant to bouncing is compressive rather than tensile, the latter being much smaller for loose materials. However, even a tensile strength equal to the smallest of all these S values would be large enough to exceed self-gravity as the main adhesive force (see also Section 4.3 and Table 3) except for *very* large bodies. However, the effective strength of many bodies to resist globally disruptive forces is often set by cracks and flaws which reduce the overall effective S to near zero, with 'zero-strength' 'rubble piles' of icy boulders or even sand heaps held together solely by self-gravity. A good example is that invoked to explain the ready breakup of some sun-grazing comets and of Shoemaker–Levy 9 by Jupiter (Asphaug & Benz 1994). We denote this class of body (self-gravity exceeding strength globally) as 'loose'.

In Section 4.3, we will argue that the high tidal gravity gradients around WD stars are so large that inside the classical Roche limit – which is far ($x \sim 100$) from the WD – they act to pull apart bodies of all sizes but only down to the limit of their constituent parts in which internal strength exceeds self-gravity. In other words bodies break up into parts bounded by their low-strength internal fault surfaces but no further at that stage. The infalling assembly of this processed debris will now comprise objects of a wide range of sizes but each of much higher integrity (and tensile strength) than its parent. In this region, strength rather than self-gravity becomes the opponent of tidal fragmentation, with sublimative mass-loss also limiting fragmentation to large bodies only (See Section 5). In this inner sublimation region, we will consider two broad classes of infalling matter strength: 'weak' (like comet nucleus matter) and 'strong' (rock) once again using the format $S = S_{\rm snow} \times [S/S_{\rm snow}]$ and $S = S_{\rm rock} \times [S/S_{\rm rock}]$ for snowy and rocky bodies, respectively, with fiducial values in numerical expressions of $S_{\rm snow} = 10^{4}$ and $S_{\rm rock} = 10^{10}$ dyne cm^{-2}, respectively. The six order-of-magnitude range in S values across debris types is a major factor in our findings, although an even wider range can be included in our modelling equations simply by adjusting $S/S_{\rm rock}$ or $S/S_{\rm snow}$ appropriately.

3.6 Orbital geometry and speed

Brown et al. (2011) and Brown et al. (2015) argued that, except in the very final stages of interaction with the deep atmosphere (when reached), or possibly in cases of rapid fragmentation (Sekanina & Kracht 2015), the centre of mass of an infalling solid body pretty much follows the locus and velocity of a Keplerian parabolic orbit about the central star. Brown et al. (2011) and Brown et al. (2015) considered the general case of a parabola with arbitrary periastron distance q (which also defines the stellar surface entry angle for cases where $q < R_\star$).

In this paper, we are concerned with the behaviour of infalling material at the opposite extreme from the slow inflow of accretion disc matter as viscosity redistributes angular momentum – namely the case of infallers having orbital eccentricities near unity and very small perihelion distances q close to or less than $R_{\rm WD}$ (with very low angular momentum). We will loosely term all of these *impactors* but intend to include both those that could actually impact the atmosphere (star plungers or divers) and those that would have near-miss fly-bys (star grazers) *if* they are not fully sublimated or fragmented before getting that close. For such objects, along most of their path inside the Roche limit ($x \sim 100$) down to x of a few, the trajectory and velocity are nearly identical to those of a linear parabolic orbit ($q = 0$). Through the next two sections, we consider them as such to simplify the mathematical treatment of the sublimation/fragmentation processes (see also Brown et al. 2011) who treat exactly the case of general q. In Section 6, we allow for the effect of deviations from the linear parabolic trajectory in addressing the behaviour (entry angle, etc.) of material actually impacting the WD surface and in Section 7 how near-miss star-grazing material might find its way on to the surface.

In the regime ($r \gg R_{\rm WD}$) of the linear parabola approximation, the only component of the velocity vector is the radial speed $v(r) = v_r(r) = \dot{r} = {\rm d}r/{\rm d}t$ with the property that

$$\frac{{\rm d}v}{{\rm d}t} \equiv \dot{v} = v\frac{{\rm d}v}{{\rm d}r} = -\frac{GM_*}{r^2} \tag{8}$$

yielding (for $v(r \to \infty) = 0$) the usual solution

$$v(r) = \left(\frac{2GM_\star}{r}\right)^{1/2} = v_\star\left(\frac{R_\star}{r}\right)^{1/2}. \tag{9}$$

4 PROCESSES OF DESTRUCTION OF INFALLING BODIES

4.1 Overview

As noted above, destruction of infalling bodies occurs by a combination of: (a) sublimative mass-loss by an energy flux F of starlight that is sufficiently large to raise the bodies above the vaporization temperature of at least some, and eventually all, of their components; (b) fragmentation due to the stellar tidal or possibly internal pressure forces exceeding the internal strength and self-gravity of the body and (c) frictional ablative mass-loss and ram-pressure pancaking and deceleration effects in the dense low atmosphere.

The importance of these various processes all decline with distance r but at differing rates. Stellar radiation flux (sublimation) declines as $\propto 1/r^2$ while tidal forces decline faster as $\propto 1/r^3$ and effectively cut-off at a finite distance when self-gravity and body strength offset them. Finally, atmospheric frictional ram-pressure effects vary as $\sim \rho_{\rm atm}(r)$ where the atmospheric mass density $\rho_{\rm atm}(r) \propto \exp(-(r-R_*)/H)$ near $r = R_*$ with scaleheight $H \ll R_*$. Consequently, these only become important within a few H of $r = R_{\rm WD}$. Disruptive internal pressure is also only important if very high mass-loss rates arise near the star (e.g. Sekanina & Kracht 2015).

We then argue (in Section 4.3.2), by analogy with observations of fragmentation of some sun grazers and of SL-9 by Jupiter and the modelling of the latter by Asphaug & Benz (1996), that the initial process is tidal disruption of large very loose structures into smaller more robust components in which strength everywhere exceeds self-gravity.

Thereafter as infall progresses from large r, radiative sublimation dominates until fragmentation sets in (if at all) or bow-shock ablation/deceleration takes over near the photosphere. Below we therefore first model (Section 4.2) the infall evolution of $a(r)$ and $M(r)$ assuming that only sublimation is active. Then, in Section 4.3 we discuss the basics of tidal fragmentation and (see also Bear & Soker 2015) include the effects of strength as well as of self-gravity. The latter is often ignored but in fact proves to be dominant even for *quite* weak snowy cometary material as we show below. Then, in Section 5 we discuss the interplay of sublimation and tidal fragmentation as a function of original infaller size. We determine the spatial and parametric ranges for which tidal fragmentation may dominate over sublimation, drawing conclusions relevant to the WD debris infall problem. We defer to Section 6 treatment of the details of destruction of objects (*impactors*) which are large/strong enough to enter the high-density gas layers low in the atmosphere where destructive hydrodynamic effects abruptly take over from sublimation and tidal forces. In Section 7.1, we briefly discuss the issues involved in whether and how sublimated atomic/molecular matter and fragmented pebbly/dusty debris can reach the stellar surface and in Section 7.2 what happens to original infallers or to their fragmented pieces. These pieces would be close to but not quite in the regime of direct infall, but rather they have orbits grazing close by the photosphere – specifically we address how they may shed enough of their angular momentum to reach the photosphere.

One other destructive force proposed (in the solar comet context) as sometimes important in infalling debris deposition is (Steckloff et al. 2015) the ram pressure $P_{\rm ramsub}$ of sublimating mass outflow when that outflow is high (near the star). Based on the rates found by Brown et al. (2011) or the equations of the next subsection, one finds that for comets quite near the sun, $P_{\rm ramsub}$ can exceed the low strength S of cometary, but not that of rocky, material. However, Gundlach et al. (2012) argued that if the outflow is symmetric enough, the inward reaction force to the outflow pressure $P_{\rm ramsub}$ can *oppose* fragmentation. On the other hand, Sekanina & Kracht (2015) have invoked an energetic exothermal process in ice crystal formation to explain the sudden fragmentation of Comet C/2012 S1 Ison while still well outside the Roche lobe. Such processes may have to be considered for some stellar infall but we omit them here as their importance is not yet widely agreed upon by the community.

4.2 Sublimation in starlight

By taking the infalling body to have near zero albedo, the heating power of starlight entering the infalling body is $a^2 F_{\rm rad}$, with the stellar radiation flux $F_{\rm rad}$ is given by equation (4).[2] We also neglect radiative cooling, assuming that the sublimation occurs on a timescale faster than that of radiative energy loss. This neglect is based on the fact that the specific energy $\mathcal{L} \sim 2.6 \times 10^{10}$ erg g^{-1} $\sim$0.01 eV per nucleon needed for sublimation of ice and rock is much smaller than that needed to heat it to the radiative equilibrium $T_{\rm eq} \sim T_*/x^{1/2}$ viz $kT_{\rm eq}/m_{\rm p} \sim 0.6/x^{1/2}$ eV. An exception occurs at $x \gg 1$, where, in any case $T_{\rm eq}$ falls below the sublimation threshold temperature and little sublimation occurs. Then, for a body of density ρ and latent heat $\mathcal{L}$, with mass $M(r)$, and size $a(r)(\rightarrow M_0, a_0$ as $r \rightarrow \infty)$, the mass-loss per unit radial distance is, using equations (8) and (9),

$$\frac{{\rm d}M}{{\rm d}r} = \frac{1}{v(r)}\frac{{\rm d}M}{{\rm d}t} = \frac{1}{v_\star}\left(\frac{r}{R_\star}\right)^{1/2}\frac{F_{\rm rad}a^2}{\mathcal{L}}$$
$$= \frac{\sigma T_\star^4}{\mathcal{L}v_\star\rho^{2/3}}\left(\frac{R_\star}{r}\right)^{3/2}M^{2/3}. \quad (10)$$

By using $M_0 = \rho a_0^3$, $M = \rho a^3$ and $v_* = (2GM_*/R_*)^{1/2}$, we obtain a solution for the variation with relative distance $x = r/R_*$ of size and mass a, M (with original incident values a_0, M_0)

$$a(x) = a_{\rm sub}(x) = a_0 - \frac{A}{x^{1/2}} \quad (11)$$

$$\frac{M(x)}{M_0} = \left(\frac{a(x)}{a_0}\right)^3 = \left(1 - \frac{A}{a_0 x^{1/2}}\right)^3 \quad (12)$$

$$A = \frac{2R_\star\sigma T_\star^4}{3\rho\mathcal{L}v_\star} = \frac{2^{1/2}R_\star^{3/2}\sigma T_\star^4}{3\rho\mathcal{L}G^{1/2}M_\star^{1/2}}, \quad (13)$$

where the *sublimation parameter* A (cm) is clearly the minimum initial size a_0 of object needed to just survive sublimation alone down to the photosphere ($r = R_*$, $x = 1$) and represents a crucial value in the debris deposition problem.

An important result of equation (11) is that in the absence of fragmentation the sublimative drop in size $a(x)$ at x is $A(x)$ independent of a_0 and in particular the size $a(1)$ of an unfragmented object reaching the photosphere is

$$a(1) = a_0 - A. \quad (14)$$

For a general star characterized by M_*, R_*, T_*, we can rewrite (13) as

$$A_\star = \left(\frac{2^{1/2}\,{\rm R}_\odot^{3/2}\sigma{\rm T}_\odot^4}{3\rho\mathcal{L}G^{1/2}\,{\rm M}_\odot^{1/2}}\right)\left[\frac{(R_\star/{\rm R}_\odot)^{3/2}\,(T_\star/{\rm T}_\odot)^4}{(M_\star/{\rm M}_\odot)^{1/2}}\right]. \quad (15)$$

For any WD star that is characterized by $M_{\rm WD}$, $T_{\rm WD}$, by using the $R_{\rm WD}(M_{\rm WD})$ relationship (1), we obtain the following expression:

$$A_{\rm WD} = \left(\frac{2^{1/2}\,{\rm R}_\odot^{3/2}\sigma{\rm T}_\odot^4}{3\rho\mathcal{L}G^{1/2}\,{\rm M}_\odot^{1/2}}\right)\gamma^{3/2}\left[\frac{(T_{\rm WD}/{\rm T}_\odot)^4}{(M_{\rm WD}/{\rm M}_\odot)}\right]. \quad (16)$$

This relation leads to the following numerical expressions for general stars and for WD stars. Each group is given in two distinct forms: one expressed in terms of values of ρ, $\mathcal{L}$, S relative to our fiducial values for rock and the other relative to our fiducial values for snow. In the WD cases, we have replaced $(T_{\rm WD}/{\rm T}_\odot)$ by $(T_{\rm WD}/10^4\,{\rm K})$ as

[2] We neglect here the correction factor $\sim$1–2 that is strictly required in equation (4) as r comes close to R because at that location the stellar radiation flux is not unidirectional, but rather arises from the large finite angular size stellar disc.

the latter is more convenient to the WD community. These fiducial values are all given in Table 3.

$$A_\star^{\rm rock}({\rm cm}) = \left(\frac{2.0\times10^2}{(\rho/\rho_{\rm rock})(\mathcal{L}/\mathcal{L}_{\rm rock})}\right)\left[\frac{\left(\frac{R_\star}{\rm R_\odot}\right)^{3/2}\left(\frac{T_\star}{\rm T_\odot}\right)^4}{\left(\frac{M_\star}{\rm M_\odot}\right)^{1/2}}\right] \tag{17}$$

$$A_\star^{\rm snow}({\rm cm}) = \left(\frac{3.7\times10^3}{(\rho/\rho_{\rm snow})(\mathcal{L}/\mathcal{L}_{\rm snow})}\right)\left[\frac{\left(\frac{R_\star}{\rm R_\odot}\right)^{3/2}\left(\frac{T_\star}{\rm T_\odot}\right)^4}{\left(\frac{M_\star}{\rm M_\odot}\right)^{1/2}}\right] \tag{18}$$

$$A_{\rm WD}^{\rm rock}({\rm cm}) = \left(\frac{1.8}{(\rho/\rho_{\rm rock})(\mathcal{L}/\mathcal{L}_{\rm rock})}\right)\left[\frac{\left(T_{\rm WD}/10^4\,{\rm K}\right)^4}{\left(M_{\rm WD}/{\rm M_\odot}\right)}\right] \tag{19}$$

$$A_{\rm WD}^{\rm snow}({\rm cm}) = \left(\frac{33}{(\rho/\rho_{\rm snow})(\mathcal{L}/\mathcal{L}_{\rm snow})}\right)\left[\frac{\left(T_{\rm WD}/10^4\,{\rm K}\right)^4}{\left(M_{\rm WD}/{\rm M_\odot}\right)}\right]. \tag{20}$$

The second expression ($A_\star^{\rm snow}$) agrees numerically with the results of the Brown et al. (2011) paper on solar comets for $M_* = {\rm M_\odot}$, $R_* = {\rm R_\odot}$ in the case of zero periastron.

The above two expressions for $A(T)$ in our fiducial WD cases are shown in Fig. 1.

By comparing the value of A given by equation (15) for the sun with that from equation (16) for a WD of the same mass and temperature, we see that an object 1000 times smaller can survive sublimation down to the surface of the WD compared to the size needed to reach the surface of the sun. This result is due to the fact that although the sublimating starlight has the same flux near the stellar surface in both cases, the effective time of exposure to that flux scales as the infall time $R_\star/v_\star \propto R_\star^{3/2}$ which is $\gamma^{3/2} = 10^{-3}$ times smaller for a WD than for the sun. In order for the minimum incident $a_o = A$ value to allow an object to survive to the photosphere to be the same as for the sun, the WD of the same mass would have to be hotter than the sun by a factor $10^{3/4}$ or $T_{\rm WD} \approx 32\,600$ K. For smaller WD masses, the minimum size for survival increases, partly because of R. Hence, infall time is larger, but also because the luminosity $\propto R^2$, and so sublimative mass-loss increases.

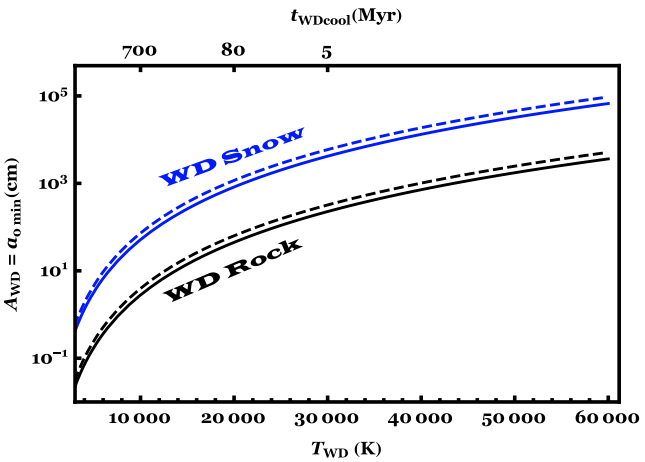

Figure 1. Plot of $A_{\rm WD}$ versus $T_{\rm WD}$ in the range $3000 < T_{\rm WD}({\rm K}) < 60\,000$ for rocky (lower pair of lines) and snowy (upper pair of lines) fiducial parameters and for masses $M_{\rm WD} = 0.4,\ 0.8\,{\rm M_\odot}$ (dashed and solid curves). Note that $A_{\rm WD} = a_{0\rm min}$ the minimum incident size needed to survive sublimation alone (no fragmentation) down to the WD surface. The top axis shows the mean cooling time $t_{\rm WDcool}$ (for an average $M_{\rm WD}$ value) corresponding to the values of $T_{\rm WD}$ along the bottom axis. $t_{\rm WDcool}(a_{0\rm min})$ is thus the time after which objects of initial size $a_{0\rm min}$ can just reach the surface without total sublimation.

4.3 Tidal fragmentation including material strength

4.3.1 General case

Neglecting internal pressure forces, the net disruptive force ($\mathcal{F}_{\rm tot}$) across a small infalling body (size a) is the difference between the disruptive tidal force ($\mathcal{F}_{\rm T}$), and the sum of the binding self-gravity ($\mathcal{F}_{\rm G}$) and tensile strength ($\mathcal{F}_{\rm S}$) forces. (The following summary of forces is similar to that in Bear & Soker 2015 within factors of order unity.)

$$\mathcal{F}_{\rm tot} = +|\mathcal{F}_{\rm T}| - |\mathcal{F}_{\rm S}| - |\mathcal{F}_{\rm G}|\,. \tag{21}$$

Standard approximations for each component are

$$\mathcal{F}_{\rm T} \approx \frac{GM_\star Ma}{2r^3}, \tag{22}$$

$$\mathcal{F}_{\rm G} \approx -\frac{GM^2}{a^2}, \tag{23}$$

$$\mathcal{F}_{\rm S} = -Sa^2. \tag{24}$$

The condition for a body to remain intact is thus (replacing M by ρa^3 and setting $M_\star = 4\pi\rho_\star R_\star^3/3$) that a should satisfy

$$\frac{|\mathcal{F}_{\rm S}+\mathcal{F}_{\rm G}|}{\mathcal{F}_{\rm T}} = \frac{S/(G\rho^2a^2)+1}{M_*/(2\rho r^3)} = \frac{S/(G\rho^2a^2)+1}{(2\pi/3)(\rho_\star/\rho x^3)} \geq 1 \tag{25}$$

which defines the maximum size $a_{\rm frag}$ of object that can avoid fragmentation at distance $r = xR_*$ namely

$$a(x) \leq a_{\rm frag}(x) = \sqrt{\frac{S/G\rho^2}{(2\pi/3)(\rho_\star/\rho x^3)-1}}. \tag{26}$$

In this paper, we will mainly be discussing the properties of this equation in the limit where the strength S term dominates over self-gravity – see Section 4.3.3 – but first we look at the opposite low S limit of 'loose' incoming material held together only by self-gravity, which was mentioned already in Sections 3.1 and 3.5.

4.3.2 The loose (zero S*) self-gravity-dominated Roche-limit regime*

In the (loose) limit,

$$\mathcal{F}_{\rm S}/\mathcal{F}_{\rm G} \ll 1. \tag{27}$$

Equation (25) simplifies to the usual Roche limit form

$$x > x_{\rm Roche} = \left(\frac{2\pi\rho_{\rm WD}}{3\rho}\right)^{1/3} = \frac{1}{\gamma}\left(\frac{2\pi\rho_\odot}{3\rho}\left(\frac{M_{\rm WD}}{\rm M_\odot}\right)^2\right)^{1/3} \tag{28}$$

which means typically $r_{\rm Roche} = \gamma x_{\rm Roche} R_{\rm WD} \sim 100 R_{\rm WD} \sim 1\,{\rm R_\odot}$. This result is expected because the gravity gradient of a $1\,{\rm M_\odot}$

WD is the same as that of the sun at the same absolute distance, regardless of the size of the object concerned, so long as it is *loose* with self-gravity dominating over strength.

As already mentioned in Sections 3.1 and 3.5, many incident debris object are likely initially to be *loose* in the sense of being aggregates of smaller more internally solid pieces, or permeated by cracks or other faults. The *global* strength of such objects against disruption of its loose components can be very small, far less than the *internal* strengths of the latter (Asphaug & Benz 1996). We thus envisage the scenario that all debris approaching a WD within around 100 WD radii will tend to be tidally fragmented into smaller component volumes containing matter of much greater integrity and with global strength much higher than that of the object as a whole and than self-gravity. Inward of this distance the effects of tides on the remnant objects will be dependent on the greater strength S of their material, be it *weak* or *strong*, as well as on distance x, as we analyse in Section 4.3.3. This scenario is just what we observed for Shoemaker–Levy 9 as it approached Jupiter (Asphaug & Benz 1996). The above equations show that the strength S needed in an object of size a and density ρ for strength to dominate over self-gravity is only $S > G\rho^2 a^2 = 175(a\,(\mathrm{km}))^2$ (dyne cm^{-2}) for the density of snow and $6300(a\,(\mathrm{km}))^2$ for the density of rock. These S values are very small except for large objects (km and up).

4.3.3 *The weak and strong* S*-dominated regime*

When we now consider equations (24) and (25) for *large* S, we recall that fragmentation onset is no longer solely a function of the infaller distance x and density as in the loose (*rubble pile*) Roche limit case, but also of the infaller strength S and size a. We find the condition on $a(x)$ to avoid fragmentation is

$$a(x) < a_{\mathrm{frag}}(x) = \sqrt{\frac{S/G\rho^2}{(2\pi/3)(\rho_\star/\rho x^3 - 1)}} \approx Bx^{3/2}, \tag{29}$$

where

$$B = \sqrt{\frac{3S}{2\pi G\rho\rho_\star}} = \sqrt{\frac{2SR_\star^3}{G\rho M_\star}}. \tag{30}$$

The final expression amounts to neglecting self-gravity as opposed to strength and is a good approximation whenever $\rho_* \gg \rho x^3$. Later results show that for WDs, this approximation is valid except for *very* large, weak and low-density infallers. Essentially it amounts to dropping the -1 from the denominator of equation (29), which arose from the self-gravity term $\mathcal{F}_\mathrm{G}$. It emphasizes the fact, not widely appreciated, that even for materials of low S like snowy cometary nuclei, self-gravity $\mathcal{F}_\mathrm{G}$ is unimportant compared to material strength $\mathcal{F}_\mathrm{S}$ in opposing tidal fragmentation except for quite large objects. This can be seen by examining the ratio

$$\mathcal{R} = \frac{\mathcal{F}_\mathrm{G}}{\mathcal{F}_\mathrm{S}} = \frac{G\rho^2 a^2}{S} \tag{31}$$

$$\mathcal{R}_{\mathrm{rock}} = 0.6\frac{(\rho/3\ \mathrm{g\,cm^{-3}})^2(a/\,1000\,\mathrm{km})^2}{(S/10^{10}\ \mathrm{dyne\,cm^{-2}})} \tag{32}$$

$$\mathcal{R}_{\mathrm{snow}} = 0.017\frac{(\rho/0.5\ \mathrm{g\,cm^{-3}})^2(a/\,1\,\mathrm{km})^2}{(S/10^{4}\ \mathrm{dyne\,cm^{-2}})}. \tag{33}$$

In Table 4, we show $\mathcal{R}_{\mathrm{rock}}$ and $\mathcal{R}_{\mathrm{snow}}$ versus a(cm). For our fiducial cometary value of $S = 10^4$ dyne cm^{-2} (Table 4), the size has to exceed about 1 km (mass around 10^{15} g, as in C/2011 W3 Lovejoy) for self-gravity to dominate over strength, while for $S = 10^3$ dyne cm^{-2}, the minimum size is around 100 m. For rocks with our fiducial $S = 10^{10}$ dyne cm^{-2}, the minimum is around 1000 km which is why only asteroids/dwarf planets larger than this size tend towards sphericity (isotropic self-gravity defeats anisotropic rock strength). The relevance of the classical Roche tidal limit (based on self-gravity alone) is solely for the disassembling of aggregations of bodies that are very loosely bound or unbound (apart from by self-gravity) such as rubble or sand piles. It is not relevant to scales on which the constituent bodies (individual boulders, sandgrains, ice crystals etc.) have integrity in the sense of significant internal strength with no weak fracture planes, as already mentioned in Sections 3.1 and 3.5.

Table 4. Ratio of forces of self-gravity to internal strength.

Type	a (cm)	$\mathcal{R}$
Rock	10^2	6.0×10^{-13}
Rock	10^3	6.0×10^{-11}
Rock	10^4	6.0×10^{-9}
Rock	10^5	6.0×10^{-7}
Rock	10^6	6.0×10^{-5}
Snow	10^2	1.7×10^{-8}
Snow	10^3	1.7×10^{-6}
Snow	10^4	1.7×10^{-4}
Snow	10^5	1.7×10^{-2}
Snow	10^6	1.7

B (cm) is clearly a *binding size parameter* measuring the threshold size that must be exceeded for the tidal force to overcome its strength and thus for fragmentation to set in. It is also obviously the minimum size of object which would fragment if placed directly at $x = 1$. By considering equation (29), we can also see that B can be expressed in terms of the relative distance $x = (a_o/B)^{2/3}$ at which a body of initial size a_o would start to fragment in the absence of any significant sublimative reduction in size (i.e. in the limit of very small A due, for example, to very large $\mathcal{L}$ or low T_{WD}). In reality, as we discuss in Section 5, one must consider the interplay of the processes with sublimative decline of $a(x)$ allowing deeper infall before fragmentation.

Thus, for a general star we can write

$$B_\star = \sqrt{\frac{2SR_\star^3}{G\rho M_\star}} = \sqrt{\frac{2S\mathrm{R}_\odot^3}{G\rho\,\mathrm{M}_\odot}}\frac{(R_\star/\mathrm{R}_\odot)^{3/2}}{(M_\star/\mathrm{M}_\odot)^{1/2}}. \tag{34}$$

By using the $R(M)$ relation for WDs, in their case it becomes

$$B_{\mathrm{WD}} = \gamma^{3/2}\sqrt{\frac{2\mathrm{R}_\odot^3}{G\mathrm{M}_\odot}}\left(\frac{S}{\rho}\right)^{1/2}\frac{1}{(M_{\mathrm{WD}}/\mathrm{M}_\odot)}. \tag{35}$$

The corresponding numerical values for rock and snow infallers to stars and to WDs are

$$B_\star^{\mathrm{rock}}(\mathrm{cm}) = 1.3\times10^8\left(\frac{S/S_{\mathrm{rock}}}{\rho/\rho_{\mathrm{rock}}}\right)^{1/2}\frac{(R_\star/\mathrm{R}_\odot)^{3/2}}{(M_\star/\mathrm{M}_\odot)^{1/2}} \tag{36}$$

$$B_\star^{\mathrm{snow}}(\mathrm{cm}) = 3.2\times10^5\left(\frac{S/S_{\mathrm{snow}}}{\rho/\rho_{\mathrm{snow}}}\right)^{1/2}\frac{(R_\star/\mathrm{R}_\odot)^{3/2}}{(M_\star/\mathrm{M}_\odot)^{1/2}} \tag{37}$$

$$B_{\mathrm{WD}}^{\mathrm{rock}}(\mathrm{cm}) = 1.3\times10^5\left(\frac{S/S_{\mathrm{rock}}}{\rho/\rho_{\mathrm{rock}}}\right)^{1/2}\frac{1}{(M_{\mathrm{WD}}/\mathrm{M}_\odot)} \tag{38}$$

$$B_{\rm WD}^{\rm snow}({\rm cm}) = 3.2 \times 10^2 \left(\frac{S/S_{\rm snow}}{\rho/\rho_{\rm snow}}\right)^{1/2} \frac{1}{(M_{\rm WD}/{\rm M}_\odot)}. \quad (39)$$

It is evident from equations (36)–(39) that, while similar to the solar case for similar absolute r values, tidal fragmentation is far more important for WDs than for the sun for r values nearing the stellar radius. The reason is because of the much larger stellar surface tidal force gradient ($\propto GM/R^3$ from equation 30, so a factor of 10^6 larger for a given mass). Though $B = a_{\rm frag}(x = 1)$ is the largest size of object that could be placed directly at the photosphere without fragmenting, allowing for sublimative loss of size during infall, in the absence of fragmentation, corresponds to an infalling object of initial size $a_0 = B + A$.

4.4 Destruction by atmospheric impact

As we will confirm in Section 5, regimes exist where intact incident objects (or intact components of tidally fragmented loose incident objects) partially survive sublimation down to $x \sim 1$, where they undergo destruction by *impact* with the stellar atmosphere or possibly disruptive processes in a grazing near miss. We defer detailed modelling of such cases to Section 6 after we have discussed the parameter regimes in which it, and also sublimative and fragmentational destruction, occurs.

5 DESTRUCTION PARAMETER REGIMES

5.1 Basics

In Sections 4.2 and 4.3, we have discussed separately how body size $a(x, a_0)$ declines with distance $xR_{\rm WD}$ due to sublimation alone (equation 11) and how the maximum size $a_{\rm frag}$ which can survive tidal fragmentation alone declines with x. This is all for x smaller than the boundary where tidal forces inside the Roche (self-gravity-dominated) limit have already processed very loosely bound infalling debris into smaller chunks of higher integrity in which internal strength far exceeds self-gravity. So it is clear that there is interplay between all the processes (see Sections 6 and 7). Qualitatively, it is apparent that the possible fates of a stellar infall object whose cohesion is from internal strength are as follows:

(i) Total *SUBLIMATION* outside the photosphere without encountering its tidal fragmentation limit.

(ii) Here, we lump together, under the heading *IMPACT*, both (a) actual impacts ($q < R_{\rm WD}$) and (b) very close grazing encounters (say $R_{\rm WD} < q \ll 2R_{\rm WD}$) with the photosphere before complete sublimation or reaching its fragmentation limit. Destruction in the actual impact case is by abrupt ablative mass-loss and deceleration via bow-shock interaction with the dense stellar atmosphere, as detailed in Section 6. The final fate of matter undergoing grazing near misses is discussed in Section 7 along with whether and how the products of fragmentation and of sublimation well above the photosphere eventually reach it.

(iii) *FRAGMENTATION* occurs before total sublimation or photospheric impact. It is beyond the scope of this paper to analyse in detail the behaviour of such fragmenting bodies (see also Asphaug & Benz 1996) and here we mainly refer to their initial fragmentation point as their end point as it signifies the demise of the original single bodies. However, we note that the behaviour of any of the smaller objects resulting from the first fragmentation which retain integrity (in the sense of S once again dominating over the tidal force) can be followed along the same lines as our treatment above until they either sublimate totally, impact the photosphere or reach their own fragmentation limit and fragment again. We briefly examine below some special cases of this hierarchical fragmentation. (Also, in Section 7, we touch on other processes affecting post-fragmentation evolution.)

We can shed some light here on hierarchical fragmentation theory for cases where fractional sublimative decrease in size $a(x)$ between successive fragmentations is small. This approximation applies for $B \gg A$ – for example to large enough a_0, $\mathcal{L}$ and/or low enough $T_{\rm WD}$. Then, by equation (29), an object of finite tensile strength S and size a_1 first reaches its tidal disruption limit at distance $x_1 = (a_1/B)^{2/3}$ (if $a_1 > B$ so that $x_1 > 1$). From that point onwards, one can imagine two limiting behaviours.

The first is a *marginally stable* progression in which the mass and size of the infalling body are almost steadily diminished by tidal loss of small fragments such that $a(x)$ is kept just at the limiting value $a(x) = Bx^{3/2}$ with the body mass $M(x)$ declining with x according to $M(x)/M_1 = [a(x)/a_1]^3 = (x/x_1)^{9/2}$ and arriving at the photosphere ($x = 1$) with precisely the critical tidal disruption size B there, the rest of the mass having been transformed into small particles en route.

Secondly, at the other extreme, we can envisage each tidal disruption occurring at $x = x_1$ and subsequent critical points, if any, to take the form of breakup into j equal parts with $j \geq 2$. Then, inside x_1, the object initially comprises j parts, each of mass $M_2 = M_1/j = \rho a_1^3/j$ and size $a_2 = a_1/j^{1/3}$. If this same process repeats, with the same j value, for each of these initial j tidal disruption products when they reach $x_2 = (a_2/B)^{2/3}$ (provided $x_2 > 1$), and so on, after k such stages the original object comprises j^k pieces each of size $a_1/j^{k/3}$ at distance $x_k = (a_k/B)^{2/3}$ until $x_k < 1$ or $a_k < B$. This shows that, in this regime, regardless of the value of j, tidal fragmentation leads to arrival near the photosphere of fragments each of size close to the critical tidal disruption size B there. This means that objects of initial size $a_1 \gg B$ are all reduced to a size $\sim B$ near $x = 1$ by a fragmentation process lying somewhere between a large number k of successive splittings, each yielding a small number j of pieces, or a small number k of successive splittings, each yielding a large number j of pieces such that $j^k \sim (a_1/B)^3$.

These results indicate that for any given value of impactor parameters – especially strength S – tidal forces ensure that fragmentation will break up any object larger than a clear lower limiting size before it reaches the photosphere. In Section 6.3, we evaluate these size limits and their consequences for the depths which impactors can reach before their explosive destruction.

In this section, we want to determine in which of these fate domains, and at what end depth, the destruction of any specific infaller lies as a function of its initial incident size a_o, for specified values of its intrinsic properties (ρ, $\mathcal{L}$, S) and those of the star ($T_{\rm WD}$, $M_{\rm WD}$). It is apparent from Sections 4.2 and 4.3 that, for given a_0, there are only two controlling parameters, A and B. These parameters are given by equations (16) and (35) as simple products of powers of the properties of the infaller and of the star. The dominant (most wide-ranging) physical parameter factors are $T_{\rm WD}$ within A, whose magnitude is a measure of sublimation rate, and S within B, whose magnitude is a measure of the material binding opposing fragmentation (a high value of B indicates that fragmentation is *less likely*). In Section 5.2, we use the equations of Section 4 to establish a diagram of domains in the (A, B) plane showing where destruction modes lie. In fact because the equations are separately linear in A, B, a_o, we can condense the destruction domain diagrams for all a_o

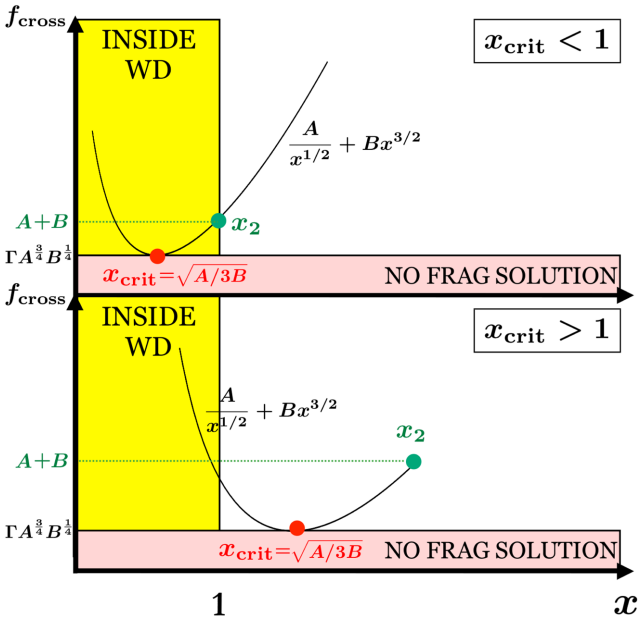

Figure 2. Recalling that $x \equiv r/R_\star$, A is the sublimation parameter and B is the binding parameter, presented here is a two-panel schematic of equation (41), showing the form of $f_{\rm cross}(x)$ for the two cases when the minimum occurs at $x_{\rm crit} < 1$ (upper panel) and $x_{\rm crit} > 1$ (lower panel) and how this form influences the position x_2 of fragmentation onset if it occurs. a_0 corresponds to a horizontal line, and fragmentation occurs if and when this line first hits the curve at a point (which may be x_1 or x_2 or neither depending on the parameters) where $x > 1$. In the red-shaded zones where $f_{\rm cross} < a_{0\rm crit} = \Gamma A^{3/4} B^{1/4}$, fragmentation cannot occur for the reasons discussed in the text.

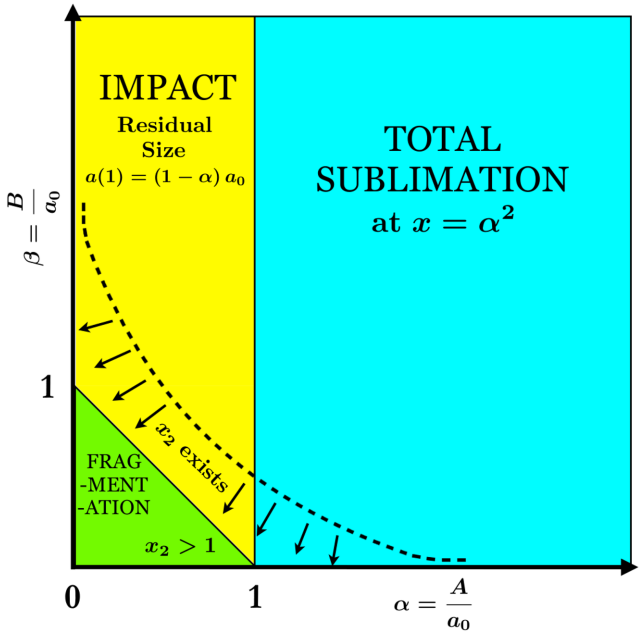

Figure 3. The three distinct domains of infaller destruction in the α, β plane – total sublimation, impact after partial sublimation, and fragmentation after partial sublimation. Fragmentation is restricted to the green triangular domain in the bottom left corner. Note that α scales as $\propto T_{\rm WD}^4/(M_{\rm WD}\rho\mathcal{L}/a_0)$ while β scales as $S^{1/2}/(\rho^{1/2}M_{\rm WD})$. Recall that $x \equiv r/R_\star$, A is the sublimation parameter and B is the binding parameter.

into a single diagram in the plane (α, β), where

$$\alpha = A/a_0$$
$$\beta = B/a_0. \tag{40}$$

5.2 Destruction domains in the (α, β) plane

We first consider in what α, β regimes fragmentation arises (i.e. in what A, B regimes for a given size a_0). As infall progresses, the ratio $a_{\rm frag}(x)/a_{\rm sub}(x)$ declines. In order for fragmentation to occur, this ratio must reach unity or less – and must do so at a value of $x > 1$ – i.e. outside the star since impact destroys the body at $x = 1$. In other words, the two $a(x)$ functions must cross, or at least touch, with fragmentation onset at some point x with x_2 the largest such x (since the infaller reaches x_2 first). The equation $a_{\rm sub}(x) = a_{\rm frag}(x)$ for such intersection can be written

$$f_{\rm cross}(x) = \frac{A}{x^{1/2}} + Bx^{3/2} = a_0, \tag{41}$$

where the crossing function $f_{\rm cross}(x)$ has a U shape – see Fig. 2 -- with a minimum value $a_{0\rm crit}(A, B)$ occurring at $x_{\rm crit}(A, B)$ where $f'_{\rm cross}(x) = 0$, namely

$$x_{\rm crit} = \left(\frac{A}{3B}\right)^{1/2} \tag{42}$$

$$a_{0\rm crit} = \Gamma \times A^{3/4} B^{1/4} = \Gamma a_0 \times \alpha^{3/4} \beta^{1/4} \tag{43}$$

with

$$\Gamma = \left[3^{1/4} + 1/3^{3/4}\right] \approx 1.75. \tag{44}$$

Turning now to the α, β plane shown in Fig. 3, using equation (43) we note that the first *necessary* condition given above for fragmentation to occur is $a_0 > a_{0\rm crit}$ which can be written $\Gamma a_0 \alpha^{3/4} \beta^{1/4} < 1$ or

$$\beta < \frac{1}{\Gamma^4 \alpha^3} = \frac{27}{256\alpha^3}. \tag{45}$$

This upper bound $\beta(\alpha)$ on fragmentation is shown as a dotted curve in Fig. 3. The second condition necessary for fragmentation to occur is that the solution x_2 of equation (41) must satisfy $x_2 > 1$. In terms of α and β, equation (41) can be written $\alpha x^{-1/2} + \beta x^{3/2} = 1$. The limiting case for fragmentation to just occur is $x_2 = 1$ such that $\alpha + \beta = 1$ or $A + B = a_o$. In other words only if

$$A + B > a_o$$
$$\alpha + \beta > 1 \tag{46}$$

can fragmentation occur above the photosphere. The meaning of this is physically simple. In the absence of fragmentation, an object of initial size a_0 would sublimate down to size $a_0 - A$ at the photosphere ($x = 1$), where the size limit for fragmentation has come down to $Bx^{3/2} = B$. Hence, only if $a_0 - A > B$ (i.e. $\alpha + \beta < 1$) can fragmentation occur before impact. This upper limiting line is also shown in Fig. 3, where we see that for all x it lies below the first limiting curve $\beta(\alpha)$ established above (though only just below at one point). So if condition (46) is satisfied then so is condition (45) and the fragmentation domain is purely the green triangular region in the bottom left corner of the (α, β) plane in Fig. 3. The significance of this triangular region is that it lies at low enough α, A (e.g. low T, high $\mathcal{L}$) that sublimation does not prevent the infaller surviving far enough in to experience strong tidal gradients. At low enough β, B (e.g. low S) the binding strength of material might not be strong enough to prevent fragmentation.

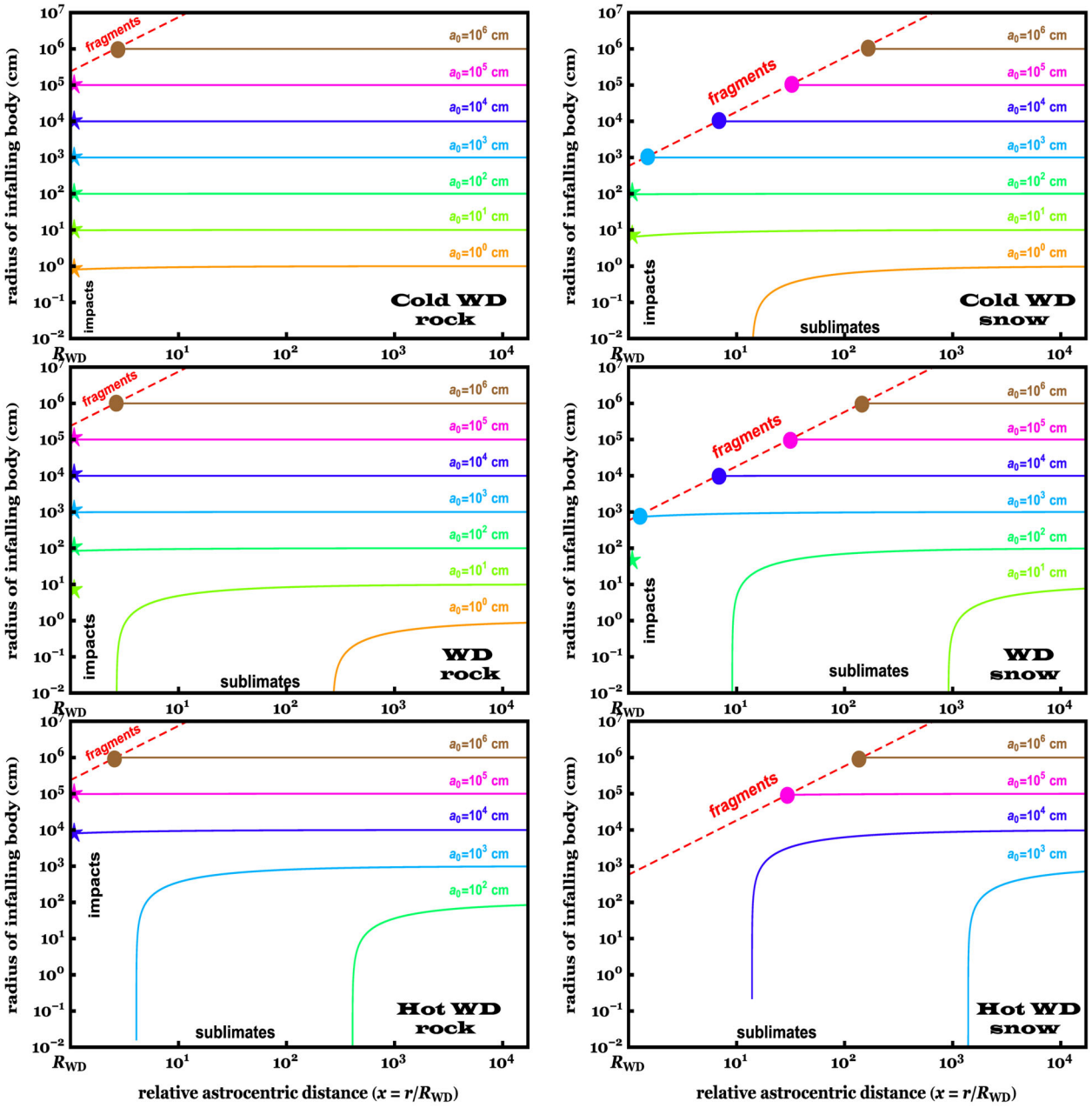

Figure 4. Size evolutions and fates for rocky (left-hand panels) and snowy (right-hand panels) bodies falling in towards a WD. Three WD temperatures are sampled (5000 K, top panels; 15 000 K, middle panels; 50 000 K, lower panels). The initial sizes of the infallers (a_0) are illustrated within each plot, and ranged from 1 to 10^6 cm. The three possible outcomes include (i) total sublimation (bottom axis), (ii) fragmentation (dashed red line) or (iii) impact with the WD photosphere (left axis).

Having established the fragmentation domain in the (α, β) plane, it is simple to divide the rest of the plane between total sublimation prior to impact and impact prior to partial sublimation. Outside of the fragmentation domain, an infaller will or will not lose its entire mass to sublimation according to whether $A > a_0$ or $A < a_0$ which means $\alpha > 1$ or $\alpha < 1$. In the first case, an infaller either is totally sublimated above the photosphere at $x = \alpha^2 = (A/a_0)^2$, or impacts the dense stellar 'surface' after being sublimatively reduced in size to $a_0(1 - \alpha)$ as shown by the α, β domains in Fig. 3.

It only remains to determine the distance $x_2 R_{WD}$ at which fragmentation sets in, if at all, for a given a_0. There are several possible approaches to this. One is to calculate and plot the sublimated size $a(x) = a_0(1 - \alpha/x^{1/2})$ for a fine grid of x values commencing at $x \gg 1$ and going down to $x = 1$ but stopping the plot at the first of the following conditions to be reached: (i) the total sublimation point $x_{sub} = \alpha^2$ where $a(x) = 0$; (ii) the fragmentation onset point $x = x_2$ where $a(x) = Bx^{3/2} = a_0\beta x^{3/2}$; (iii) impact at $x = 1$ with $a = a(1) = 1 - \alpha$. In Fig. 4, we show such plots for a set of fiducial parameters: rocky and snowy infallers (left-hand and right-hand panels), and cool, warm and hot WDs (top, middle and bottom rows), all for $M_{WD} = 0.6\,M_\odot$.

If one only wants the fragmentation point value x_2 and not the full trajectory $a(x)$, then an alternative approach is to solve numerically

Table 5. x_2 values corresponding to (α, β) pairs, where α is on y-axis and β is on the x-axis.

	$10^{-3.0}$	$10^{-2.7}$	$10^{-2.3}$	$10^{-2.0}$	$10^{-1.7}$	$10^{-1.3}$	$10^{-1.0}$	$10^{-0.7}$	$10^{-0.3}$	$10^{0.0}$
$10^{-6.0}$	100	63	34	22	14	7.4	4.6	2.8	1.7	1.0
$10^{-4.0}$	100	63	34	22	14	7.4	4.6	2.8	1.7	NA
$10^{-2.0}$	100	63	34	22	14	7.3	4.6	2.8	1.7	NA
$10^{-1.0}$	99	63	34	21	13	7.2	4.5	2.7	1.6	NA
$10^{-0.7}$	99	62	33	21	13	7.0	4.3	2.5	1.5	NA
$10^{-0.3}$	97	61	32	20	12	6.4	3.9	2.2	1.1	NA
$10^{0.0}$	93	57	30	18	11	4.9	2.2	NA	NA	NA

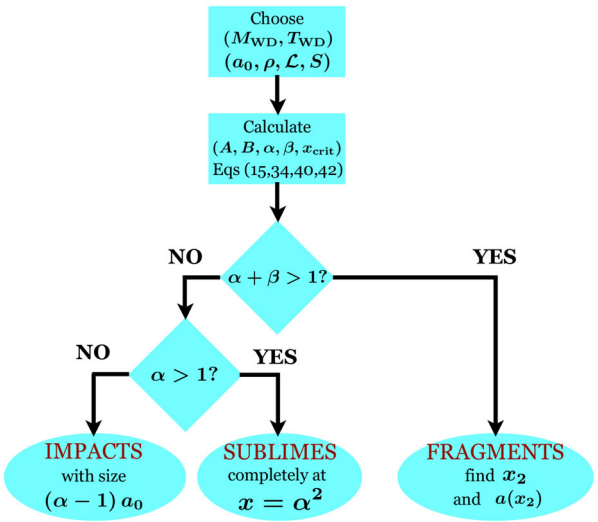

Figure 5. Schematic flow chart of how to determine the mode and position of destruction of any infaller for any WD star starting from adopted values of the physical parameters of each.

the equation $\alpha/x_2^{1/2} + \beta x_2^{3/2} = 1$ for $x_2(\alpha, \beta)$ over a large grid of α, β values, and use these as a look-up source of x_2 values or as the basis of a plot of $x_2(\alpha, \beta)$. This plot could either be a set of smooth curves of $x_2(\alpha)$ for a series of discrete β values, or as a plot of iso-x value contours on the (α, β) plane. Here, we have adopted the look-up grid option – shown as the matrix $\mathbf{X2}_{\beta,\alpha}$ – in Table 5 of values x_2 for logarithmically spaced steps in the ranges $10^{-3} \leq \beta \leq 1$ and $10^{-6} \leq \alpha \leq 1$.

Fig. 5 provides, in terms of parameters A and B, a flowchart of how to determine the fate of an infaller of size a_0.

5.3 Summary

The essence of our destruction domain results in terms of numerical values of physical parameters can best be illustrated by looking at our typical examples for parameters with our fiducial values of ρ, $\mathcal{L}$, S for rock and snow, namely

(i) *FRAGMENTATION* occurs if $\alpha + \beta < 1 \rightarrow a_0 > A + B$ which, using equations (19), (20), (38) and (39) for our fiducial rock and snow cases imply, respectively,

$$\frac{1.3 \times 10^5}{M_{\rm WD}/{\rm M}_\odot}\left[1 + 1.4 \times 10^{-5}\left(\frac{T_{\rm WD}}{10^4\,{\rm K}}\right)^4\right] < a_{0\rm rock}({\rm cm}) \qquad (47)$$

and

$$\frac{3.2 \times 10^2}{M_{\rm WD}/{\rm M}_\odot}\left[1 + 0.10\left(\frac{T_{\rm WD}}{10^4\,{\rm K}}\right)^4\right] < a_{0\rm snow}({\rm cm}). \qquad (48)$$

(ii) On the other hand, if $a_0 < A + B$ and $a_0 > A$ i.e.

$$\frac{1.8T_4^4}{M_{\rm WD}/{\rm M}_\odot} < a_{0\rm rock}({\rm cm}) < \frac{1.3 \times 10^5}{M_{\rm WD}/{\rm M}_\odot}\left[1 + 1.4 \times 10^{-5}\left(\frac{T_{\rm WD}}{10^4\,{\rm K}}\right)^4\right] \qquad (49)$$

or

$$\frac{33T_4^4}{M_{\rm WD}/{\rm M}_\odot} < a_{0\rm snow}({\rm cm}) < \frac{3.2 \times 10^2}{M_{\rm WD}/{\rm M}_\odot}\left[1 + 0.10\left(\frac{T_{\rm WD}}{10^4\,{\rm K}}\right)^4\right] \qquad (50)$$

then *IMPACT* occurs before fragmentation or complete sublimation while if $a_0 < A$ (and so $a_0 < A + B$ too) i.e.

$$a_{0\rm rock}({\rm cm}) < \frac{1.8T_4^4}{M_{\rm WD}/{\rm M}_\odot} \qquad (51)$$

or

$$a_{0\rm snow}({\rm cm}) < \frac{33T_4^4}{M_{\rm WD}/{\rm M}_\odot}, \qquad (52)$$

then *SUBLIMATION* is complete before fragmentation or impact.

These results are shown graphically in Figs 6(a) and 6(b) for rock and for snow, respectively, with the fiducial reference values of the various parameters given in Table 3.

6 THE ACTUAL 'STELLAR IMPACT' REGIME: BOW-SHOCK ABLATIVE DESTRUCTION

6.1 Background – comparison with solar debris impacts

Our description here of the destruction of bodies actually directly impacting WD photospheres is based on an extension of the Brown et al. (2015) analysis of sun-impacting comets. The case of non-compact stars in general can be similarly treated by a suitable generalization of parameters from the solar case.

Our results above show that regimes exist in which infallers (or fragments of them) can arrive near the photosphere ($r - R_{\rm WD} \ll R_{\rm WD}$) of WDs without being fragmented or fully vaporized by sublimation in starlight. The crucial property of this region of WD atmospheres is that, because of the very high gravity g and the moderate temperature T_*, the star has a very small density scaleheight (equation 6): $H \sim$ 10–100 m $\preceq 10^{-2}R_{\rm WD}$. The kinetic energy flux of the incident atmospheric flow for atmospheric mass density ρ_a is $\sim\rho_a(r)m_p v_o^3/2$, which increases exponentially with decreasing r on distance scale H. The incident radiation flux causing sublimation $F_{\rm rad} \sim 6 \times 10^{11}(T_{\rm WD}/10^4)^4$ erg cm^{-2} s^{-1} varies very slowly (length-scale $\sim R_{\rm WD}$) along the path of the infaller – roughly $\propto 1/r^2$, where

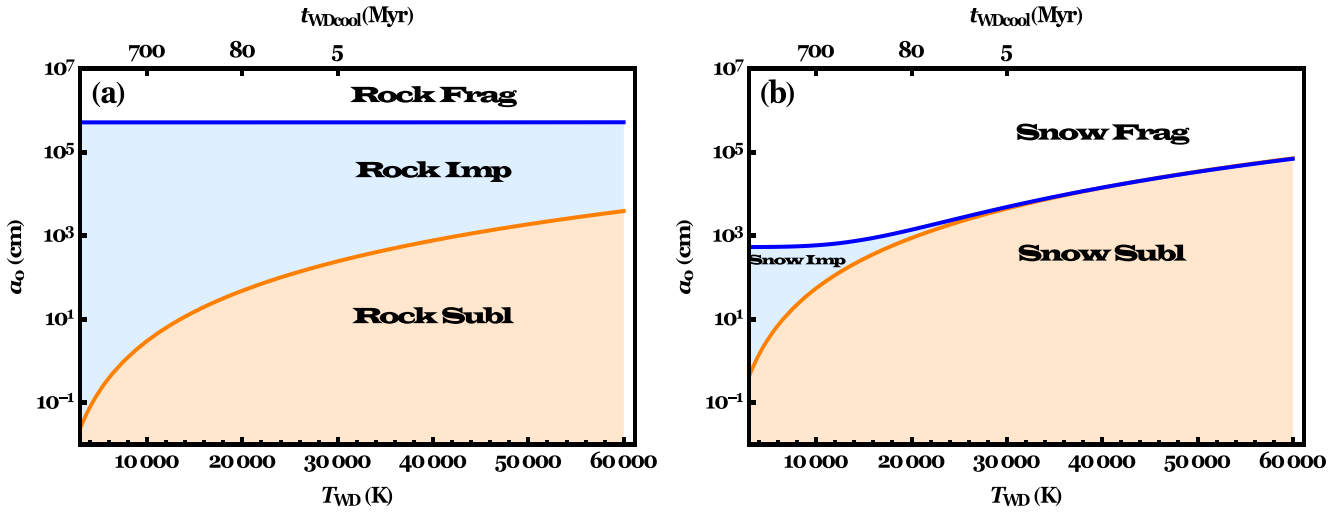

Figure 6. Temperature dependence of destruction regimes in terms of $a_0(T_{WD})$ for (a) rocky and (b) snowy bodies with the fiducial reference values of infaller parameters ρ, $\mathcal{L}$, S given in Table 3. These show that for solid rock only objects larger than several km undergo fragmentation, with impact after partial sublimation being the dominant fate in the mm – several km range for the coolest WDs, while for the hottest WDs total sublimation occurs for sizes up to around 10 m with impact occurring for larger objects up to over 1 km. For weak snowy material, for WDs of well below 30 000 K, objects over a few metres fragment and only objects below a few cm sublimate fully before fragmenting. However, above 30 000 K, total sublimation dominates for all sizes under about 1 km. Even for the coolest WDs only snowy objects in the few mm to 10 m range manage to impact before sublimating fully or fragmenting.

$r \approx R_{WD}$. Thus, as infall proceeds, atmospheric frictional heating very rapidly exceeds radiative. In order to assess the atmospheric density $\rho_a^{subtoab}$, where the crossover occurs from radiative sublimation to atmospheric ablation, we first note that only a small fraction C_H of the total incident atmospheric bombardment flux $\rho_a(r)m_p v_o^3/2$ actually reaches the nucleus and ablates it. The remainder goes into heating the atmosphere through a standoff bow shock which decelerates the impacting body and ablates the nucleus by radiative, conductive and convective heat transfer. For $C_H = 10^{-2}C_{H-2}$ (see below), the ablating energy flux is $F_{ab} \sim 10^{-2}C_{H-2}\rho_a(r)v_o^3/2 \sim 10^{24}\rho_a C_{H-2}$. This equals the radiative sublimation flux F_{rad} quoted above when $\rho_a \sim \rho_a^{subtoab} \sim 6 \times 10^{-13}$ g cm^{-3} $\times$ $(T_{WD}/10^4)^4$ or a proton number density $n_a^{subtoab}(\mathrm{cm}^{-3}) \sim 3.5 \times 10^{11}$ cm^{-3} $\times$ $(T_{WD}/10^4)^4$ [for further details, please see Brown et al. 2011. Thereafter the impactor is very rapidly destroyed by ablation and deceleration within a few vertical scaleheights H as we describe below by analogy with Brown et al. (2015).

Whether or not the impactor is fully ablated before being fully decelerated or vice versa depends on the speed v_o of the impactor. This speed determines the shock temperature and hence the heat transfer coefficients, according to the dimensionless parameter $X = 2Q/C_H v_0^2$, where large X cases refer to the deceleration-dominated regime and small X cases refer to the ablation-dominated regime. Here, $Q \gg \mathcal{L}$ is an effective latent heat describing the total energy needed to vaporize ($\mathcal{L}$) and remove 1 g of impactor material (see Brown et al. 2015). In the case of debris impacting Solar system planets, it is usually argued (e.g. Chyba et al. 1993; MacLow & Zahnle 1994; Zahnle & MacLow 1994) that the heating efficiency $C_H \propto 1/X$ is so small that X is large and the main energy lost to the body is not ablative mass-loss but simply shock heating of the atmosphere by deceleration of the body. Brown et al. (2015) have argued convincingly that, for the very high shock temperatures involved in the solar case, namely 0.4 MK for $v_0 = v_\odot = 620$ km s^{-1}, the big increase in thermal conductivity over slow planet impact shocks means that the heating efficiency is increased (X much reduced) and ablation dominates over deceleration. For WD stars ($v_{WD} \approx$ 6200 km s^{-1}), the shock temperature ≈40 MK. This conclusion – that ablation will dominate over deceleration – is even stronger so below we follow Brown et al. (2015) in assuming ablative destruction dominates and in the following we use a typical fiducial value of 10^{-2} for the uncertain parameter $X = 10^{-2}X_{-2}$. However, unlike Brown et al. (2015) we have to distinguish the behaviour of strong (rocky) bodies from weak (snowy) bodies. Brown et al. (2015) only discussed the latter, and in the solar context, whereas strong infalling rocks may behave differently in their response to atmospheric bow-shock ram pressure, specifically depending on whether or not the infalling object's cross-sectional area is enhanced by compressional pancaking.

The ram pressure of the atmosphere impinging on an infalling body is $P_{ram} = \rho v_0^2 \sim 4 \times 10^{17}\rho_a$ dyne cm^{-2} for typical WD v_0 values. A high enough ρ_a value can exceed the compressive strength of the body (which we take to be roughly comparable with the tensile strength S) and result in the body *pancaking* (Chyba et al. 1993; MacLow & Zahnle 1994; Zahnle & MacLow 1994) along its path. For this to happen requires $P_{ram} > S$ or $\rho_a^{PramoverS} > 2 \times 10^{-14}$ for S_{snow} and 2×10^{-8} for S_{rock}. Comparing these $\rho_a^{PramoverS}$ with those for $\rho^{radtoab}$, we see (see also Brown et al. 2015) that for weak (e.g. snowy cometary bodies) P_{ram} starts to drive pancaking before ablation takes over from sublimation so that pancaking is occurring through the ablation phase and the analytic bolide description (e.g. Chyba et al. 1993; MacLow & Zahnle 1994; Zahnle & MacLow 1994) applies to the pancaking. On the other hand for strong rocky bodies impacting on WDs, this is not the case so hard rocks will not pancake significantly in the WD impact ablation regime, except perhaps for the very hottest WDs.

An additional factor which can be important in the impact regime is the angle θ of incidence (to the vertical) of the infalling object. At distances well outside the star, this angle has little effect on results and we have ignored it up till now, taking θ as always small (i.e. vertical infall and periastron distance $q = 0$). However, for non-zero q, at distance r, θ is given by $\mu = \cos\theta = \sqrt{1 - q/r}$ so that for q near R_*, θ can be a large angle with $\mu \ll 1$. The reason that small μ is so important in the impact regime is that the distance over which the

atmospheric density $\rho_{\rm A}$ exponentiates *along the impacting object path* is not H but H/μ, reducing vertical penetration by a factor μ. We therefore include μ as a factor in our impact destruction depth estimates below.

We also note that, from the observability viewpoint, Brown et al. (2015) describe the result of comet–sun impacts as *cometary flares* because of the very impulsive and local energy deposition and generation of radiation signatures like impulsive X-ray bursts and generation of helio-(astero-) seismic ripples (see Winget & Kepler 2008 for a discussion of WD asteroseismology). For WD impacts, the impulsivity will be much greater because of the high impact speed and small-scale height. Specifically the encounter speed $v_{\rm WD} = (2GM_{\rm WD}/R_{\rm WD})^{1/2} \sim 10 \times v_\odot$, while the atmospheric density scaleheight $H = 2kT/\bar{m}g$ is smaller by a factor $>10^4$ for $M_{\rm WD} \approx {\rm M}_\odot$ and $T_{\rm WD} \approx {\rm T}_\odot$. The other major difference from the case of sun-plunging comets is that the surface debris arrival (i.e. escape) speed is around 10 times higher, namely $\sim$6000 km s^{-1} for 1 M$_\odot$ and the specific impact energy $\sim 10^4$ times higher, namely $\sim 2 \times 10^{19}$ erg g^{-1} or 10 MeV per nucleon (capable of producing emissions up to gamma-ray energies). In terms of total energy, a 1 km infaller at this speed has a kinetic energy of 2×10^{34} erg, or 10–100 times that of the largest solar flares ever observed. The power release in impact by an infaller of size a_0 is $\mathcal{E} \sim a_0^3 \rho v_0^2/2 > 10^{32} a_0^3$ (km) erg in a time-scale of a few times $\Delta t \sim H/v_0 < 10^{-4}$ s, corresponding to an instantaneous power $\mathcal{P} \sim \mathcal{E}/\Delta t \sim 10^{36} a_0^3$ (km) erg s^{-1} which is (very briefly) 10^3 times the bolometric luminosity $\pi R_{\rm WD}^2 \sigma T_{\rm WD}^4$ of the very hottest (60 000 K) WD stars.

Therefore, it is important to assess the observability of such impacts by their transient emissions, the discovery of which would be as exciting as the discovery of shredded planet debris orbiting near the $100R_{\rm WD}$ Roche limit via their transient absorption features (Vanderburg et al. 2015).

6.2 Destruction depths for strong (rock) and weak (snow) WD impactors

In the following, we approximate the size of the object arriving in the lower atmosphere as being a_0, i.e. that of the original incident object. When an impact occurs after small fractional sublimation ($A \ll a_0$) and no fragmentation, this is quite adequate but if sublimation has significantly reduced a_0 to say $a = a_{\rm impact} = a_0 - A$, then a_0 in the following expressions should be replaced by $a_{\rm impact}$.

6.2.1 *Expression for WD scaleheight* H

For all but the coolest WDs, we can use the fully ionized hydrogen expression (6) for the hydrostatic density scaleheight of the atmosphere which is (see also Section 2.4)

$$H_{\rm WD}({\rm cm}) = \frac{2kT_{\rm WD}}{GM_{\rm WD}m_{\rm p}/R_{\rm WD}^2} = \gamma^2 H_{\odot 4} \frac{T_{\rm WD}}{10^4\,{\rm K}} \left(\frac{{\rm M}_\odot}{M_{\rm WD}}\right)^{5/3} = 6 \times 10^3 \frac{T_{\rm WD}}{10^4\,{\rm K}} \left(\frac{{\rm M}_\odot}{M_{\rm WD}}\right)^{5/3}, \quad (53)$$

where $H_{\odot 4}$ is the scaleheight for solar surface gravity (2.7×10^4 cm s^{-2}) combined with $T = 10^4$ K. We have used relationship (1) for $R_{\rm WD}(M_{\rm WD})$.

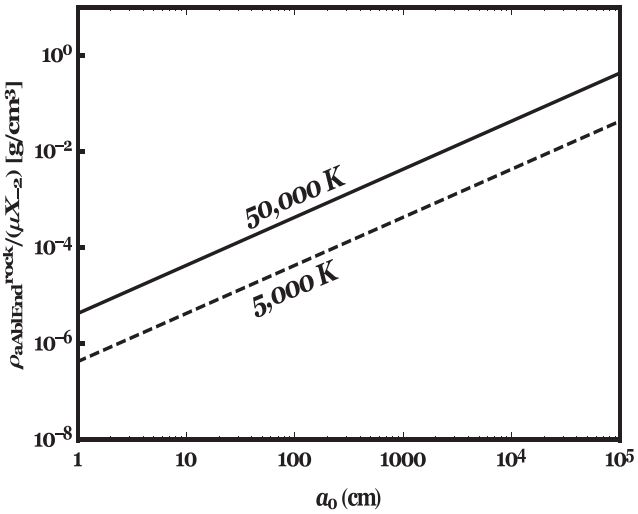

Figure 7. The WD atmospheric mass density (g cm^{-3}) $\rho_{\rm aAblEnd}^{\rm rock}/\mu X_{-2}$ versus a_0 at the terminal impact point of infalling rocks for hot and cold fiducial values of $T_{\rm WD}$, each for two values of $M_{\rm WD}$. Strong rocks do not undergo the ram-pressure-driven pancaking suffered by weaker bodies like snow. The ρ-axis has been scaled relative to the factor μX_{-2} from equation (55).

6.2.2 *Strong/rock impactors*

In the case of vertical entry of a body with no pancaking, we define the vertical atmosphere column mass density at which ablative destruction occurs as Σ_a (g cm^{-2}). We take this to be where the kinetic energy $C_{\rm H}\Sigma_a v_o^2/2$ delivered per unit area (with $\Sigma_a = H\rho_a$) equals the total energy $Q\rho a_o$ needed to drive total mass-loss per unit impactor area $M/a_0^2 = \rho a_0$. Allowing for non-vertical entry at angle $\theta = \cos^{-1}\mu$, it follows that most of the destruction occurs over a few vertical scaleheights at a *vertical* depth

$$\Sigma_{\rm aAblEnd}^{\rm rock}({\rm g\,cm^{-2}}) = \mu X \rho a_o \approx 3 \times 10^{-2} \mu X_{-2} a_o({\rm cm}), \quad (54)$$

where we have used the fiducial value $\rho = 3$ g cm^{-3} for rock. The corresponding hydrogen column number density is $N_{\rm aAblEnd}^{\rm rock}({\rm cm^{-2}}) = \Sigma_{\rm aAblEnd}^{\rm rock}/m_p \sim 2 \times 10^{22} \mu X_{-2} a_0({\rm cm})$.

The continuum optical depth (for Thomson cross-section $\sigma_{\rm T} \sim 7 \times 10^{-25}$ cm^2) is $\tau = N_a \sigma_{\rm T} \sim 0.01 \mu X_{-2} a_o({\rm cm})$, so the destruction occurs near the continuum photosphere $\tau = 1$ for vertical impact of metre (100 cm) sized objects.

The corresponding atmospheric mass density $\rho_= \Sigma_a/H$ is

$$\rho_{\rm aAblEnd}^{\rm rock}({\rm g\,cm^{-3}}) \approx \frac{5 \times 10^{-6} \mu X_{-2}}{T_{\rm WD}/10^4\,{\rm K}} \left(\frac{M_{\rm WD}}{{\rm M}_\odot}\right)^{5/3} a_0({\rm cm}), \quad (55)$$

where we have used the above expression for H as a function of $T_{\rm WD}$, $M_{\rm WD}$. The corresponding hydrogen number density is $n_{\rm aAblEnd} = \rho_{\rm aAblEnd}/m_{\rm p}$. This relation is illustrated in Fig. 7.

6.2.3 *Weak/snow impactors*

We have argued that for WD stars and low-strength impactors, the ablation-dominated regime of approximate analytic (ram-pressure-driven) impactor pancaking radius solution discussed by e.g. Chyba et al. (1993), MacLow & Zahnle (1994) and Zahnle & MacLow (1994) applies. However, we note that it depends on the condition $a_o \ll H$ and so may only be approximate for the largest bodies and coolest (smallest H) WDs that we consider. According to that

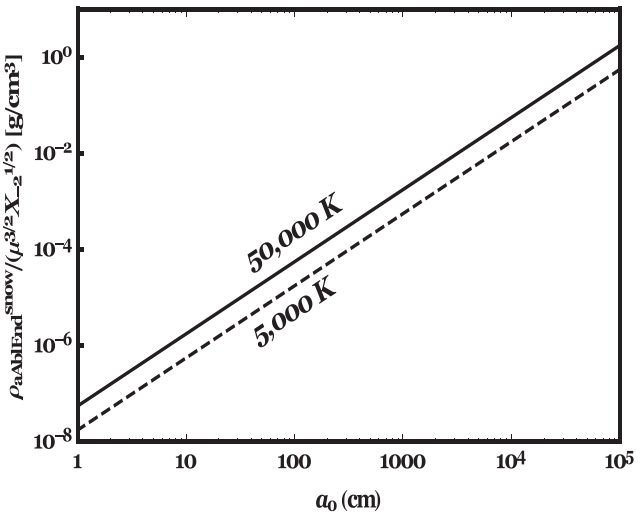

Figure 8. The WD atmospheric mass density (g cm^{-3}) $\rho_{\rm aAblEnd}^{\rm rock}/\mu X_{-2}$ versus a_0 at the terminal impact point of infalling snowy bodies for hot and cold fiducial values of $T_{\rm WD}$, each for two values of $M_{\rm WD}$. Snowy (soft) bodies undergo ram-pressure-driven pancaking. The ρ-axis has been scaled relative to the factor $\mu^{3/2}X_{-2}^{1/2}$ from equation (57).

pancaked solution, (Brown et al. 2015, page 7, their equation 26), the atmospheric mass column density $\Sigma_a(r) = \int_r^\infty \rho_{\rm a}\, {\rm d}r$ (g cm^{-2}) at which ablative mass, momentum and energy loss peak sharply and destroy the impactor is given by

$$\Sigma_{\rm aAblEnd}^{\rm snow} = \left(\frac{\mu^3\rho^2 a_0^3 X}{\pi H}\right)^{1/2}$$
$$= 3.6\times10^{-4}({\rm g\,cm^{-2}})\frac{\mu^{3/2}X_{-2}^{1/2}}{(T_{\rm WD}/10^4\ {\rm K})^{1/2}}\left(\frac{M_{\rm WD}}{{\rm M}_\odot}\right)^{5/6} a_0^{3/2}({\rm cm}) \quad (56)$$

and the mass density is

$$\rho_{\rm aAblEnd}^{\rm snow} = 6\times10^{-8}\frac{\rm g}{\rm cm^3}\frac{\mu^{3/2}X_{-2}^{1/2}}{(T_{\rm WD}/10^4\ {\rm K})^{1/2}}\left(\frac{M_{\rm WD}}{{\rm M}_\odot}\right)^{5/6} a_0^{3/2}({\rm cm}), \quad (57)$$

where we have again used the above expression for $H(T_{\rm WD}, M_{\rm WD})$ (see Fig. 8). The dependences on μ, X, T, a_o are all more complex than in the strong rock case above because of the effects the pancaking has on the weaker material. Estimating the optical depth τ in the same way as for the rocky body case, we find that even vertically entering snowy bodies would explode above the photosphere unless they are larger than ∼1000 cm.

6.3 Effect of fragmentation size limit on maximum impactor depths

We saw in Section 4.3 that tidal fragmentation sets upper limits to the sizes ($a(1) = B$) of rocky and snowy objects which can exist intact at the photosphere (equations 38 and 39). These in turn set upper limits to the maximum depths at which explosive destruction at rocky and snowy bodies can occur. By inserting these two equations into equations (54) and (56), we obtain the following tidally limited values, using our fiducial values for rock and snow parameters

$$\Sigma_{\rm aAblEndMax}^{\rm rock}({\rm g\,cm^{-2}}) \approx 4\times10^3\mu X_{-2}\left(\frac{M_{\rm WD}}{{\rm M}_\odot}\right)^{-1} \quad (58)$$

and

$$\Sigma_{\rm aAblEndMax}^{\rm snow} = 2({\rm g\,cm^{-2}})\frac{\mu^{3/2}X_{-2}^{1/2}}{(T_{\rm WD}/10^4\ {\rm K})^{1/2}}\left(\frac{M_{\rm WD}}{{\rm M}_\odot}\right)^{-2/3}. \quad (59)$$

The corresponding electron scattering optical depths $\tau = \Sigma\sigma_{\rm T}/m_{\rm p} \sim 0.4\Sigma$ are

$$\tau_{\rm aAblEndMax}^{\rm rock} \approx 1600\mu X_{-2}\left(\frac{M_{\rm WD}}{{\rm M}_\odot}\right)^{-1} \quad (60)$$

and

$$\tau_{\rm aAblEndMax}^{\rm snow} = 0.8\frac{\mu^{3/2}X_{-2}^{1/2}}{(T_{\rm WD}/10^4\ {\rm K})^{1/2}}\left(\frac{M_{\rm WD}}{{\rm M}_\odot}\right)^{-2/3}. \quad (61)$$

These equations tell us that (for $X = 0.01$) the largest rocky bodies (10^5 cm) arriving at the star unfragmented explode below the photosphere ($\tau = 1$) provided their entry angle cosine $\mu > 10^{-3}$ and that a vertically entering rock needs only be ∼100 cm in size to do so. On the other hand, even the largest snowy bodies (300 cm) arriving at the star unfragmented and vertically will explode above the photosphere at $\tau \sim 0.8$.

7 DISCUSSION AND CONCLUSIONS

7.1 Discussion

All of the processes we have modelled above deposit the mass of individual steep fast infallers along their trajectories in the form of : sublimation products – ions, atoms, molecules and some intermingled small dust particles, too refractory and efficiently cooled to sublimate initially; in some cases, tidal fragmentation products (dust, pebbles, small boulders) with enhanced total mass sublimation rate because of the increased surface to mass ratio. Any unsublimated remains of the original object or of its fragments will ultimately either impact the photosphere or graze close by it. Apart from the direct stellar impact case, none of the processes we have modelled directly result in metallic debris deposition *on* the WD surface (the *tabula rasa*), where the metals are seen spectroscopically. Although the details of metal accretion are beyond the scope of this paper, here we briefly discuss below some of the issues that require further work to answer the question of how such final deposition comes about. We also recall our conclusion (Section 4.3, equations 38–39) that tidal disruption limits the maximum size of chunks that can ever arrive near the photosphere, namely of order 1 km for rocky and 3 m for snowy bodies.

7.1.1 Detectability and temporal signature of individual impactors

We saw in Section 6 that the deposition of the mass and kinetic energy of impactors is extremely localized (scale of order scaleheight H) and impulsive (time-scale of order H/v_o). This initial impact would cover a tiny fraction of the stellar disc and so be very hard to see in absorption, though its very high temperature would likely yield a briefly detectable flash of XUV emission. Furthermore, the exploding debris would spread across the stellar disc in seconds and might then be visible in absorption. We have shown that any individual impacting object is limited in size by tidal fragmentation to about 1 km if rocky and about 3 m if snowy, such objects containing

masses $\sim 3 \times 10^{15}$ g and $\sim 10^{7}$ g, respectively, or $\sim 10^{39}$ and $\sim 10^{31}$ nucleons, respectively. Spread over the whole area $\sim 10^{19}$ cm^2 of a WD these correspond to column densities of 10^{20} and 10^{12} nucleons cm^{-2} or $10^{20}/\mathcal{A}$ and $10^{12}/\mathcal{A}$ for species of atomic mass $\mathcal{A}$. Even for line transitions of moderate absorption cross-section $\sim 10^{-17}$ cm^2, the optical depth is large $\sim 1000/\mathcal{A}$ for the largest (1 km) rocky bodies and easily detectable in high-resolution spectroscopy (Zuckerman et al. 2007; Koester et al. 2014) while even for the largest (3 m) snowy impactors the optical depth is $\sim 10^{-5}/\mathcal{A}$ and potentially within the reach of precision spectrometry while it lasts. The duration of detectability depends on the type (DA or DB) of WD star involved and requires further work to assess, but along lines of argument like the following.

In the case of hydrogen-rich (DA-type) WD atmospheres, which are primarily radiative, the diffusive time-scale for fresh contaminant matter to sink out of sight is only days to weeks (10^{5-6} s) which would be roughly the detectability duration of a metallicity enhancing impact. For a single 1 km (3×10^{15} g) rocky impactor, the mass sinkage rate over that period is $\sim 10^{9-10}$ g s^{-1}, roughly similar to the range estimated by Bergfors et al. (2014) as the steady rate needed to sustain the observed level of surface contamination. Consequently to sustain the metallicity signature quasi-steadily would require arrival of 1 km rocks at intervals of days to weeks, or smaller masses more frequently. If the mean mass supply rate were delivered as bursts of 1 km objects at longer intervals, the metallicity time signature would be intermittent rather than quasi-steady.

For helium-rich convective DB-type WD stars, the situation is quite different and more complex due to their atmospheres being convective which has major effects: (i) the convective downflow will remove surface debris and spread it through the convection zone in hours. Therefore, apart from that very brief transient, the contamination will not be visible until enough material has arrived to spread throughout the convection zone; (ii) convective upflow greatly increases the time (to Myr) for sinkage out of the convection zone. Thus, the metallicity signature once established would persist for Myr after a cut-off in debris supply.

7.1.2 *Near-miss star-grazing chunks*

These are the residual post-sublimation parts of steep infallers, or of their tidally fragmented pieces, which come close to impact but have $q > R_{\rm WD}$, and so orbit the star. We have seen in Section 4.3 that tidal forces limit the size of such star grazers to around 1 km for rocky and 3 m for snowy debris. The question of how these can ultimately end up as photospheric contaminants boils down to how they can shed their small angular momentum. This could occur by a variety of processes including mutual collisions, Poynting Robertson drag (most effective for the smallest pieces), or, most likely, by quite rapid sublimation. A 1 km object in a 6000 K radiation field like that at the surface of the sun or of a 6000 K WD would sublimate totally in a matter of hours. In an elliptical orbit extending from near the WD surface out to the Roche distance, that time is increased by roughly the ratio of the orbital period to the time $R_{\rm WD}/v_0$ spent near the star: a factor of ~ 1000, while it is shortened by a factor of 10^4 for very hot WDs ($T_{\rm WD} \sim 10 {\rm T}_\odot$). Thus, the process of eccentric orbital decay and infall of boulders quickly becomes that of orbital decay of dust, atoms and ions.

7.1.3 *Radiation forces on dust*

Residual material from infallers which have fully sublimated above the photosphere ($x > 1$) will likely be in the form of molecules, atoms and ions plus some dust particles, the proportions of each depending on competing processes such as sputtering, dissociation and ionization versus accretion, and molecular/atomic recombination. Such small particles will in general start in different gravitational orbits from their progenitor infalling rocks and ice but also be subject to forces additional to those discussed in Section 4 such as radiation pressure, Poynting–Robertson drag and Yarkovsky effects, which can either aid or inhibit descent of material on to the WD surface.

(i) *Radiation pressure (RP)*: for a particle of effective radiation cross-section d^2 (cm^2) and mass M (g), the ratio of radially outward radiation pressure to radially inward gravitational force is (neglecting finite disc correction factors near the star)

$$\Phi = \frac{R_{\rm WD}^2 \sigma T_{\rm WD}^4}{G M_{\rm WD} c} \frac{d^2}{M} = \frac{{\rm R}_\odot^2 \sigma T_{\rm WD}^4}{G {\rm M}_\odot c} \gamma^2 \left(\frac{{\rm M}_\odot}{M_{\rm WD}} \right)^{5/3} \frac{d^2}{M}$$
$$= 7 \times 10^{-8} \left(\frac{{\rm M}_\odot}{M_{\rm WD}} \right)^{5/3} \frac{d^2}{M} \left(\frac{T_{\rm WD}}{10^4 \, {\rm K}} \right)^4, \quad (62)$$

where we have used the $R_{\rm WD}(M_{\rm WD})$ relations (equations 1 and 2) and have assumed that the dust particles are much larger than the effective wavelength of the starlight viz $\sim 400 \, {\rm nm}/(T_{\rm WD}/10^4 \, {\rm K})$.

Whether or not a particle can be prevented by radial radiation pressure from settling on to the star thus depends on the factor $T_{\rm WD}^4 \times d^2/m$ which we discuss here for dust and below for ions and atoms. For pebbles and dust particles of density ρ (a few g cm^{-3}), $d^2/m \sim 1/\rho d$ (cm^2 g^{-1}), so that in this case

$$\Phi = \Phi_{\rm dust} \approx \frac{2 \times 10^{-8}}{d({\rm cm})} \left(\frac{T_{\rm WD}}{10^4 \, {\rm K}} \right)^4 \left(\frac{{\rm M}_\odot}{M_{\rm WD}} \right)^{5/3}. \quad (63)$$

Consequently, even for WD stars that are as hot as 60 000 K, only for infalling dust particles of residual size after radiative sublimation $d < 10^{-5}$ cm (0.1 μm) would radiation pressure defeat gravity and drive particles outward. For larger particles of the same density, the radial force of radiation pressure is small compared to the inward force of gravity. However, larger particles than these are subject to the additional:

(i) *Poynting–Robertson effect* (*P-R drag*, Burns, Lamy & Soter 1979) of the radiation field, namely the transverse drag it exerts on the motion of orbiting matter which causes it to fall inward even when the radial radiation pressure force on them is much less than gravity. Its importance depends on the size of the object and is very different for the WD case compared to the solar (Rafikov 2011a,b; Veras et al. 2015b) because of different temperatures at different distances from the stars. For a detailed discussion of this effect and others, see Wyatt & Whipple (1950), Burns et al. (1979), Bonsor & Wyatt (2010), Rafikov (2011b) and Veras, Eggl & Gänsicke (2015a). However, a rough estimate of the force involved for transverse orbital speed u is that it is the transverse force of the radiation field incident at aberrational angle u/c. Then, the transverse equation of motion is

$$\frac{{\rm d}u}{{\rm d}t} = -\frac{d^2}{M} \frac{u}{c} P_{\rm rad} = u \frac{d^2}{M} \frac{\sigma T_{\rm WD}^4}{c^2} \quad (64)$$

which implies an orbital decay time from distance $xR_{\rm WD}$ of

$$\tau_u \sim \frac{u}{{\rm d}u/{\rm d}t} \sim \frac{M}{d^2} \frac{c^2 x^2}{\sigma T_{\rm WD}^4}$$
$$\sim 70 \, {\rm yr} \frac{\rho x^2 d({\rm cm})}{(T_{\rm WD}/10^4)^4} \sim 6 \, {\rm d} \frac{\rho x^2 d({\rm microns})}{(T_{\rm WD}/10^4)^4}. \quad (65)$$

This rough estimate suggests that for pebble-sized infallers, the P-R drag time-scale is months to millennia, whereas for micron-sized dust, the time-scale is minutes to months. The proportionalities in this estimate match previous formulations, whereas the numerical coefficient is dependent on several factors (see Veras et al. 2015a), such as reflection efficiency and absorption efficiency. Another factor is eccentricity of the orbit, which necessitates the solution of coupled differential equations. Highly eccentric orbits can generate infall time-scales that differ by several orders of magnitude (see e.g. fig. 1 of Veras et al. 2015b), basically because (as in the above case of sublimation) the process (P-R drag) only acts effectively over a small fraction of the orbit near the star.

P-R drag actually represents the consequences of a special case of more general radiation forces. As outlined by Vokrouhlický et al. (2015) for the Solar system and Veras et al. (2015a) for post-main-sequence exosystems, radiation changes both an object's spin and orbit. Spin-inducing changes are known as the YORP effect. This effect is particularly important if an object is spun up to breakup speed, an outcome which has been starkly observed in the Solar system (Harris 1994; Jacobson et al. 2014). Orbital acceleration due to radiation is a combination of absorption, re-emission from immediate reflection and re-emission from delayed reflection. The first two aspects together comprise RP and P-R drag, whereas the sometimes-neglected third aspect creates the Yarkovsky effect (Radzievskii 1954; Peterson 1976). Veras et al. (2015a) demonstrated that the Yarkovsky effect can induce changes that are several orders of magnitude stronger than the P-R drag, but 'turns on' only for objects larger than pebbles. Consequently, P-R drag probably remains the most important radiation-based effect for debris within a few Roche radii of a WD.

7.1.4 Radiation pressure effect on infalling atoms and ions

Except for the coolest WDs, or for cases of very high matter infall rate and density, we would expect the ionizing radiation field close to the star to overwhelm recombination. Consequently, most gaseous products of sublimation are likely to be in a fully or highly ionized state. For an ionized H atom (p,e pair) one can use $M \approx m_{\rm p} = 1.7 \times 10^{-24}$ g and d^2 of order the Thompson cross-section $\sigma_T \sim 7 \times 10^{-25}$ cm^2, giving $\Phi < 7 \times 10^{-5}$ for any ($T_{\rm WD}$, $M_{\rm WD}$). Consequently, H-ions experience negligible RP force compared to gravity and should not be blown away by it. For heavier species, the same will be true unless the ionization is partial and involves a much larger photo-absorption cross-section d^2 (Chayer, Fontaine & Wesemael 1995; Koester et al. 2014). On the other hand, any infalling ion experiences Lorentz and pressure forces of the WD magnetic field, though these should only re-route the inflow along field lines rather than preventing it.

In the case of neutral atoms or low-ionization states, the photo cross-section d^2 can be much larger than σ_T (e.g. $\sim 10^{-15}$ cm^2 for H Lyman α) which would give $\Phi \sim 35 (T_{\rm WD}/10^4)^4 \left(\frac{\rm M_\odot}{M_{\rm WD}}\right)^{5/3}$ so that, for all but the coolest WDs, the infall of any such highly absorbing atoms would be inhibited by radiation pressure. On the other hand, however, the fraction of neutrals present decreases as the temperature increases. The relative importance of radiation pressure on atoms and ions will thus evolve as WDs age and cool.

7.2 Main conclusions

An outstanding issue in post-main-sequence planetary science is identification of the dynamical origin of metallic pollutants on WD stars in the very common case where no slow-infall accretion disc exists of sufficient mass to be detectable thus far by IR excess resulting from reprocessed starlight, nor other means. Direct or very steep infall of pollutants in near parabolic orbits of very small perihelion and angular momentum may offer one possible solution since they involve a hard-to-detect fast, and hence tenuous inflow, especially if it is near isotropic.

We have addressed, in greater depth than hitherto, the issue of what processes and parameters of the star and of the infallers govern the nature and radial distribution of deposition of such infalling debris objects as a function of their incident mass and composition and of the WD mass and temperature (cooling age). Our analysis is mainly analytic, producing simple expressions and an algorithm for easy application to modelling specific WD stars and their metallicity pollution data. Our results involve the incident size a_0 of the infaller and several of its intrinsic physical properties (density ρ, latent heat $\mathcal{L}$, tensile strength S) and on the WD mass ($M_{\rm WD}$) and effective temperature ($T_{\rm WD}$). However, for given a_0, results are a function of only two length parameters (A, B), each of which is a simple product of powers of several of the complete set of physical parameters. A is a measure of the importance of sublimation and depends most strongly on $T_{\rm WD}$ (age) while B is a measure of resistance to tidal fragmentation and is mainly determined by S.

Our analysis applies *inside* the classical Roche limit, where the stellar tidal gradient force exceeds the self-gravity of infalling objects. This force disrupts objects/structures of zero intrinsic tensile strength, such as sand or rubble piles, or objects of significant local strength that are permeated by surfaces of low or zero strength (cracks), as in the icy rubble-pile dusty-snowball models of cometary nuclei. For the typical densities of comets, asteroids and fragments thereof, the typical Roche limit is around a solar radius, or roughly 100 times a typical WD radius. Inside that all objects are tidally disrupted along all of their planes of weakness into smaller pieces, whose tensile strength is more important than self-gravity. These pieces continue their infall intact – undergoing mass-loss by sublimation – until they are completely vaporized, or impact or graze the star, or reach the point where tidal forces defeat their intrinsic strength and they fragment further.

Our equations can be applied to obtain results for a very wide range of infaller sizes and of WD and infaller parameters. Here, we have mainly shown results for four distinct regimes: cool/hot WDs, weak and volatile (snowy/comet-like) infallers and strong and refractory (rocky/asteroid-like) infallers. We have also restricted the infaller incident size range considered to be ∼cm–km. Objects originally much below cm size are totally sublimated very far out, whereas objects much above a km are scarcer and tidally fragmented further out.

Our main findings are as follows.

(i) Total sublimation above the photosphere befalls all small infallers across the whole WD temperature $T_{\rm WD}$ range, the upper threshold size rising with $T_{\rm WD}$ and 100× larger for rock than snow.

(ii) All very large objects fragment tidally regardless of $T_{\rm WD}$, the threshold for rock being $a_0 \succeq 10^5$ cm and for snow in the range $a_0 \succeq 10^3 - 3 \times 10^4$ cm over the full range of $T_{\rm WD}$.

(iii) No body can ever arrive at the surface of a WD with a residual size (after sublimation) larger than about 1 km for rocky material or about 3 m for snowy material since it will be tidally disrupted there.

(iv) A considerable range of a_0 avoids fragmentation and total sublimation, and impacts or grazes cold WDs, although the range narrows rapidly with increasing $T_{\rm WD}$, especially for snowy bodies.

Important future work would involve linking the results presented here with individual WDs exhibiting signatures of metal pollution in their atmospheres, and implementing a detailed deposition model resulting from debris infall. As detailed in Section 7.1, residual dust is subject to sputtering, dissociation and ionization, whereas larger fragments might be influenced by Poynting–Robertson drag, the YORP effect and the Yarkovsky effect. The effort to better understand these effects may then be traced back to the architectures and compositions of WD planetary systems which create such infall, and lead to a better understanding of planetary system evolution across all life stages.

ACKNOWLEDGEMENTS

We thank the referee for their encouraging, very helpful and constructive comments, and for rederiving all of the equations without prompting. We also thank Pier-Emmanuel Tremblay for discussions on convective turn-over times in WDs. JCB gratefully acknowledges the financial support of a Leverhulme Emeritus Fellowship EM-2012-050\4 and of a UK STFC Consolidated Grant ST/L000741/1, and thanks K Simpson for proof-reading and helpful science comments. BTG and DV benefited from the support of European Union ERC grant number 320964.

REFERENCES

Aannestad P. A., Kenyon S. J., Hammond G. L., Sion E. M., 1993, AJ, 105, 1033
Alcock C., Fristrom C. C., Siegelman R., 1986, ApJ, 302, 462
Alonso R., Rappaport S., Deeg H. J., Palle E., 2016, A&A, 589, L6
Antoniadou K. I., Veras D., 2016, MNRAS, 463, 4108
Asphaug E., Benz W., 1994, Nature, 370, 120
Asphaug E., Benz W., 1996, Icarus, 121, 225
Barber S. D., Belardi C., Kilic M., Gianninas A., 2016, MNRAS, 459, 1415
Bear E., Soker N., 2015, MNRAS, 450, 4233
Bergeron P., Wesemael F., Beauchamp A., 1995, PASP, 107, 1047
Bergfors C., Farihi J., Dufour P., Rocchetto M., 2014, MNRAS, 444, 2147
Biele J. et al., 2015, Science, 349, a9816
Bonsor A., Wyatt M., 2010, MNRAS, 409, 1631
Bonsor A., Mustill A. J., Wyatt M. C., 2011, MNRAS, 414, 930
Brown J. C., Potts H. E., Porter L. J., Le Chat G., 2011, A&A, 535, AA71
Brown J. C., Carlson R. W., Toner M. P., 2015, ApJ, 807, 165
Burns J. A., Lamy P. L., Soter S., 1979, Icarus, 40, 1
Chayer P., Fontaine G., Wesemael F., 1995, ApJS, 99, 189
Chyba C. F., Thomas P. J., Zahnle K. J., 1993, Nature, 361, 40
D'Antona F., Mazzitelli I., 1990, ARA&A, 28, 139
Davidsson B. J. R., 1999, Icarus, 142, 525
Davidsson B. J. R., 2001, Icarus, 149, 375
Debes J. H., Walsh K. J., Stark C., 2012, ApJ, 747, 148
Dennihy E., Debes J. H., Dunlap B. H., Dufour P., Teske J. K., Clemens J. C., 2016, ApJ, 831, 31
Falcon R. E., Winget D. E., Montgomery M. H., Williams K. A., 2010, ApJ, 712, 585
Farihi J., 2016, New Astron. Rev., 71, 9
Farihi J., Jura M., Zuckerman B., 2009, ApJ, 694, 805
Farihi J., Barstow M. A., Redfield S., Dufour P., Hambly N. C., 2010, MNRAS, 404, 2123
Farihi J., Koester D., Zuckerman B., Vican L., Gänsicke B. T., Smith N., Walth G., Breedt E., 2016, MNRAS, 463, 3186
Fontaine G., Brassard P., Bergeron P., 2001, PASP, 113, 409
Frewen S. F. N., Hansen B. M. S., 2014, MNRAS, 439, 2442
Friedrich S., Jordan S., Koester D., 2004, A&A, 424, 665
Gaensicke B. T. et al., 2016, ApJ, 818, L7
Gänsicke B. T., Marsh T. R., Southworth J., Rebassa-Mansergas A., 2006, Science, 314, 1908
Gänsicke B. T., Koester D., Marsh T. R., Rebassa-Mansergas A., Southworth J., 2008, MNRAS, 391, L103
Gänsicke B. T., Koester D., Farihi J., Girven J., Parsons S. G., Breedt E., 2012, MNRAS, 424, 333
Gary B. L., Rappaport S., Kaye T. G., Alonso R., Hambsch F.-J., 2017, MNRAS, 465, 3267
Greenberg J. M., Hitoshi M., Tetsuo Y., 1995, A&A, 295, L35
Gundlach B., Blum J., 2016, A&A, 589, A111
Gundlach B., Blum J., Skorov Y. V., Keller H. U., 2012, preprint (arXiv:1203.180)
Gurri P., Veras D., Gänsicke B. T., 2017, MNRAS, 464, 321
Hamada T., Salpeter E. E., 1961, ApJ, 134, 683
Hamers A. S., Portegies Zwart S. F., 2016, MNRAS, 462, L84
Harris A. W., 1994, Icarus, 107, 209
Jacobson S. A., Marzari F., Rossi A., Scheeres D. J., Davis D. R., 2014, MNRAS, 439, L95
Jura M., 2006, ApJ, 653, 613
Jura M., Xu S., 2010, AJ, 140, 1129
Jura M., Xu S., 2012, AJ, 143, 6
Jura M., Young E. D., 2014, Annu. Rev. Earth Planet. Sci., 42, 45
Kilic M., Redfield S., 2007, ApJ, 660, 641
Koester D., Gänsicke B. T., Farihi J., 2014, A&A, 566, AA34
Liebert J., Bergeron P., Holberg J. B., 2005, ApJS, 156, 47
MacLow M.-M., Zahnle K., 1994, ApJ, 434, L33
Malamud U., Perets H. B., 2016, ApJ, 832, 160
Manser C. J. et al., 2016a, MNRAS, 455, 4467
Manser C. J., Gänsicke B. T., Koester D., Marsh T. R., Southworth J., 2016b, MNRAS, 462, 1461
Melis C., Dufour P., 2017, ApJ, 834, 1
Mestel L., 1952, MNRAS, 112, 583
Mustill A. J., Veras D., Villaver E., 2014, MNRAS, 437, 1404
Panei J. A., Althaus L. G., Benvenuto O. G., 2000, A&A, 353, 970
Paquette C., Pelletier C., Fontaine G., Michaud G., 1986, ApJS, 61, 197
Payne M. J., Veras D., Holman M. J., Gänsicke B. T., 2016, MNRAS, 457, 217
Payne M. J., Veras D., Gänsicke B. T., Holman M. J., 2017, MNRAS, 464, 2557
Peterson C., 1976, Icarus, 29, 91
Petrovich C., Muñoz D. J., 2017, ApJ, 834, 116
Radzievskii V. V., 1954, Dokl. Akad. Nauk SSSR, 97, 49
Rafikov R. R., 2011a, MNRAS, 416, L55
Rafikov R. R., 2011b, ApJ, 732, LL3
Rappaport S., Gary B. L., Kaye T., Vanderburg A., Croll B., Benni P., Foote J., 2016, MNRAS, 458, 3904
Redfield S., Farihi J., Cauley P. W., Parsons S. G., Gaensicke B. T., Duvvuri G., 2016, ApJ, preprint (arXiv:1608.00549)
Sekanina Z., Kracht R., 2015, ApJ, 801, 135
Steckloff J. K., Johnson B. C., Bowling T., Jay Melosh H., Minton D., Lisse C. M., Battams K., 2015, Icarus, 258, 430
Stone N., Metzger B. D., Loeb A., 2015, MNRAS, 448, 188
Tremblay P.-E., Ludwig H.-G., Steffen M., Bergeron P., Freytag B., 2011, A&A, 531, L19
Tremblay P.-E., Ludwig H.-G., Steffen M., Freytag B., 2013, A&A, 552, A13
Tremblay P.-E., Gianninas A., Kilic M., Ludwig H.-G., Steffen M., Freytag B., Hermes J. J., 2015, ApJ, 809, 148
Tremblay P.-E., Cummings J., Kalirai J. S., Gänsicke B. T., Gentile-Fusillo N., Raddi R., 2016, MNRAS, 461, 2100
Vanderburg A. M. et al., 2015, Nature, 526, 546
Veras D., 2016a, R. Soc. Open Sci., 3, 150571
Veras D., 2016b, MNRAS, 463, 2958
Veras D., Gänsicke B. T., 2015, MNRAS, 447, 1049
Veras D., Mustill A. J., Bonsor A., Wyatt M. C., 2013, MNRAS, 431, 1686
Veras D., Leinhardt Z. M., Bonsor A., Gänsicke B. T., 2014a, MNRAS, 445, 2244
Veras D., Shannon A., Gänsicke B. T., 2014b, MNRAS, 445, 4175
Veras D., Eggl S., Gänsicke B. T., 2015a, MNRAS, 451, 2814

Veras D., Leinhardt Z. M., Eggl S., Gänsicke B. T., 2015b, MNRAS, 451, 3453
Veras D., Mustill A. J., Gänsicke B. T., Redfield S., Georgakarakos N., Bowler A. B., Lloyd M. J. S., 2016, MNRAS, 458, 3942
Veras D., Carter P. J., Leinhardt Z. M., Gaensicke B. T., 2017a, MNRAS, 465, 1008
Veras D., Mustill A. J., Gaensicke B. T., 2017b, MNRAS, 465, 1499
Veras D., Georgakarakos N., Dobbs-Dixon I., Gaensicke B. T., 2017c, MNRAS, 465, 2053
Vokrouhlický D., Bottke W. F., Chesley S. R., Scheeres D. J., Statler T. S., 2015, in Michel P., DeMeo F. E., Bottke W. F., eds, Asteroids IV. Univ. Arizona Press, Tucson, AZ, p. 509
Wilson D. J., Gänsicke B. T., Koester D., Raddi R., Breedt E., Southworth J., Parsons S. G., 2014, MNRAS, 445, 1878
Winget D. E., Kepler S. O., 2008, ARA&A, 46, 157
Wyatt S. P., Whipple F. L., 1950, ApJ, 111, 134
Wyatt M. C., Farihi J., Pringle J. E., Bonsor A., 2014, MNRAS, 439, 3371
Xu S., Jura M., Koester D., Klein B., Zuckerman B., 2014, ApJ, 783, 79
Xu S., Jura M., Dufour P., Zuckerman B., 2016, ApJ, 816, L22
Zahnle K., MacLow M.-M., 1994, Icarus, 108, 1
Zhou G. et al., 2016, MNRAS, 463, 4422
Zuckerman B., Becklin E. E., 1987, Nature, 330, 138
Zuckerman B., Koester D., Reid I. N., Hünsch M., 2003, ApJ, 596, 477
Zuckerman B., Koester D., Melis C., Hansen B. M., Jura M., 2007, ApJ, 671, 872
Zuckerman B., Melis C., Klein B., Koester D., Jura M., 2010, ApJ, 722, 725

This paper has been typeset from a TEX/LATEX file prepared by the author.